Received: 20 October 2015 | Accepted: 17 February 2017

DOI: 10.1111/gbi.12234

ORIGINAL ARTICLE

WILEY gebiology

The Neoarchaean surficial sulphur cycle: An alternative hypothesis based on analogies with 20th-century atmospheric lead

M. Gallagher[1] | M. J. Whitehouse[2] | B. S. Kamber[1]

[1]Department of Geology, School of Natural Sciences, Trinity College Dublin, Dublin, Ireland

[2]Department of Geosciences, Swedish Museum of Natural History, Stockholm, Sweden

Correspondence
M. Gallagher, Department Of Geology, School of Natural Sciences, Trinity College Dublin, Dublin, Ireland.
Email: megallag@tcd.ie

Funding information
SYNTHESYS grant, Grant/Award Number: SE-TAF-3395; the European Community – Research Infrastructure Action under the FP7 "Capacities" Specific Programme; EU FP7 Marie Curie Actions – Career Integration Grant

Abstract

We revisit the S-isotope systematics of sedimentary pyrite in a shaly limestone from the ca. 2.52 Ga Gamohaan Formation, Upper Campbellrand Subgroup, Transvaal, South Africa. The analysed rock is interpreted to have been deposited in a water depth of ca. 50–100 m, in a restricted sub-basin on a drowning platform. A previous study discovered that the pyrites define a nonzero intercept $\delta^{34}S_{V\text{-}CDT}$–$\Delta^{33}S$ data array. The present study carried out further quadruple S-isotope analyses of pyrite, confirming and expanding the linear $\delta^{34}S_{V\text{-}CDT}$–$\Delta^{33}S$ array with an $\delta^{34}S$ zero intercept at $\Delta^{33}S$ ca. +5. This was previously interpreted to indicate mixing of unrelated S-sources in the sediment environment, involving a combination of recycled sulphur from sulphides that had originally formed by sulphate-reducing bacteria, along with elemental sulphur. Here, we advance an alternative explanation based on the recognition that the Archaean seawater sulphate concentration was likely very low, implying that the Archaean ocean could have been poorly mixed with respect to sulphur. Thus, modern oceanic sulphur systematics provide limited insight into the Archaean sulphur cycle. Instead, we propose that the 20th-century atmospheric lead event may be a useful analogue. Similar to industrial lead, the main oceanic input of Archaean sulphur was through atmospheric raindown, with individual giant point sources capable of temporally dominating atmospheric input. Local atmospheric S-isotope signals, of no global significance, could thus have been transmitted into the localised sediment record. Thus, the nonzero intercept $\delta^{34}S_{V\text{-}CDT}$–$\Delta^{33}S$ data array may alternatively represent a very localised S-isotope signature in the Neoarchaean surface environment. Fallout from local volcanic eruptions could imprint recycled MIF-S signals into pyrite of restricted depositional environments, thereby avoiding attenuation of the signal in the subdued, averaged global open ocean sulphur pool. Thus, the superposition of extreme local S-isotope signals offers an alternative explanation for the large Neoarchaean MIF-S excursions and asymmetry of the $\Delta^{33}S$ rock record.

1 | INTRODUCTION

A major breakthrough in understanding the long-term evolution of the atmosphere was the discovery that mass independently fractionated sulphur (MIF-S) is preserved in sedimentary rocks older than ca. 2.4 Ga, but absent in younger strata (Farquhar, Bao, & Thiemens, 2000). In the context of experimental UV photolysis of SO_2 and atmospheric chemistry models (Farquhar, Savarino, Airieau, & Thiemens, 2001; Farquhar et al., 2000; Pavlov & Kasting, 2002), this discovery implied that extremely low free oxygen levels, less than 0.001% of the

present atmospheric concentration (Pavlov & Kasting, 2002), characterised the atmosphere before 2.4 Ga. At such low oxygen levels, the effective absence of ozone allowed for photochemical production of MIF-S in the atmosphere and its delivery to the Earth's surface. Since the discovery of MIF-S in the pre-great oxygenation event (GOE) sedimentary rock record, the combined data from many studies reveal an apparent temporal trend in the magnitude of observed $\Delta^{33}S$ anomalies (e.g., Halevy, Johnston, & Schrag, 2010; Hofmann, Bekker, Rouxel, Rumble, & Master, 2009; Thurston, Kamber, & Whitehouse, 2012). Somewhat counter-intuitively, the largest anomalies are not found in the oldest terrestrial sediments but occur in sedimentary rocks of Neoarchaean age (2.5 to 2.8 Ga), deposited only ca. 100 Ma prior to the putative GOE (e.g., Bekker et al., 2004; Farquhar & Wing, 2003; Rouxel, Bekker, & Edwards, 2005). It is worth noting that widely contrasting ranges of $\Delta^{33}S$ have been reported from time equivalent ca. 2.5 Ga old, but geographically and spatially discrete samples; the Batatal Formation in Brazil (Cheney, 1996) and the South African Campbellrand Carbonate Platform (Paris, Adkins, Sessions, Webb, & Fischer, 2014; Zhelezinskaia, Kaufman, Farquhar, & Cliff, 2014). In addition, an asymmetry in the $\Delta^{33}S$ record has emerged, with mean data skewed in favour of positive $\Delta^{33}S$ values during the ca. 2.5–2.7 Ga age window (Reinhard, Planavsky, & Lyons, 2013). The significance of the topology and reason for the asymmetry of the Neoarchaean MIF-S record are subject of active research (e.g., Farquhar et al., 2013; Halevy, 2013; Halevy et al., 2010; Hofmann et al., 2009; Ohmoto, Watanabe, Ikemi, Poulson, & Taylor, 2006; Ono, Beukes, Rumble, & Fogel, 2006) but remain to be fully established.

Preservation of the ancient atmospheric MIF-S signal in the sedimentary environment was aided by the inability of the O-depleted, pre-GOE atmosphere to oxidatively weather sulphides from land. Therefore, oceanic sulphur was not sourced from riverine run-off (Canfield, 2004; Ono et al., 2003) but instead almost exclusively derived from the atmosphere. The evaporite record suggests the pre-GOE sulphate concentration of sea water was critically low, as gypsum and anhydrite were only rarely precipitated prior to halite precipitation during evaporation prior to ca. 1.9 Ga (Grotzinger & Kasting, 1993). The discovery of MIF-S significantly strengthened earlier arguments for low oceanic sulphate levels that were based on the observation that the range in $\delta^{34}S$ is much lower in Archaean sedimentary pyrite than in Phanerozoic equivalents. The original argument for low levels of seawater sulphate in the Archaean was explained by Canfield and co-workers (Canfield, Habicht, & Thamdrup, 2000; Canfield & Raiswell, 1999; Habicht, Gade, Thamdrup, Berg, & Canfield, 2002); however, the simplicity of the logic has since been revised (e.g., Fike, Bradley, & Rose, 2015). Nonetheless, a number of recent studies have put forward several lines of evidence still pointing towards low levels of seawater sulphate in the Archaean (e.g., Crowe et al. 2014; Zhelenskaia et al. 2014). Thus, the Archaean oceanic sulphur was almost exclusively derived from volcanic emissions (Holland, 1984; Walker & Brimblecombe, 1985). In this respect, it is important to recall that the style of magmatism may have evolved throughout the Precambrian. Agreement exists that the Archaean witnessed abundant emplacement of plume-derived basalt, driven by very high temperature plumes (e.g., Kamber, 2015). However, a significant irreversible decline in oceanic Ni concentration at ca. 2.6 Ga is observed (e.g., Gallagher, Turner, & Kamber, 2015; Konhauser et al., 2009, 2015; Large et al., 2014), likely reflecting the disappearance of komatiite and high-Mg basalts on land (Kamber, 2010), a direct consequence of cooling mantle plume temperatures and a concomitant end of very high-Mg volcanism (Konhauser et al., 2009). Once plume magmas became less magnesian, the crust too was being reorganised in terms of radioactive heat production, and the geology started to acquire a more familiar look to that of the Phanerozoic (Kamber, 2015). The onset of Wilson-style plate tectonics has most recently been proposed to have occurred at ca. 3 Ga (Shirey & Richardson, 2011). For these reasons, there is a possibility that throughout the Archaean, the relative contributions of sulphur species from plume-related versus subduction volcanoes may have changed and influenced the evolution of the Neoarchaean sulphur cycle.

Here, we develop a new working hypothesis for the interpretation of the Neoarchaean S-cycle. It is based on an analogy with the 20th-century anthropogenic atmospheric Pb emission "experiment." It posits that Neoarchaean S-cycling was far more dynamic than previously thought (e.g., Fischer et al., 2014) and that seawater isotopic compositions could have fluctuated on much shorter timescales than they do today (Crowe et al., 2014), facilitating the preservation of local S-isotope signatures. We propose the possibility that non-zero intercept $\delta^{34}S_{V\text{-}CDT}$–$\Delta^{33}S$ data arrays may alternatively represent very localised S-isotope signatures in the Neoarchaean surface environment, whereby fallout from local volcanic eruptions could imprint recycled MIF-S signals into pyrite of restricted depositional environments, thereby avoiding attenuation of the signal in the subdued, averaged global open ocean sulphur pool. This model is applied to new quadruple S-isotope data and compiled triple S-isotope MIF-S data for Neoarchaean sulphides, addressing the magnitude of MIF-S, the apparent asymmetry of Neoarchaean MIF values, and linear data arrays from a single Neoarchaean sample (Figure 1a), which do not pass through the origin of the $\delta^{34}S_{V\text{-}CDT}$–$\Delta^{33}S$ plot (e.g., Kamber & Whitehouse, 2007; Whitehouse, 2013).

2 | MATERIALS

In terms of new data, this study revisits the 2.521 ± 3 Ga (Sumner & Bowring, 1996) shallow water sedimentary rocks of the Gamohaan Formation of the Campbellrand Subgroup, Transvaal Supergroup, South Africa (Beukes, 1987; Sumner & Bowring, 1996). Rocks from this Formation were first investigated for their MIF-S composition by Papineau, Mojzsis, Coath, Karhu, and Mckeegan (2005) and have since been the subject of further, more comprehensive, studies (Kamber & Whitehouse, 2007; Whitehouse, 2013). The Gamohaan Formation is the uppermost Formation of the >2 km Campbellrand Subgroup, which preserves interesting quadruple S-isotope systematics throughout (Izon et al., 2015). The Gamohaan Formation is characterised by platformal subtidal fenestral microbialites and shales that ultimately grade into the overlying deeper water Kuruman Formation iron formation (Figure 2), and has been interpreted to have formed

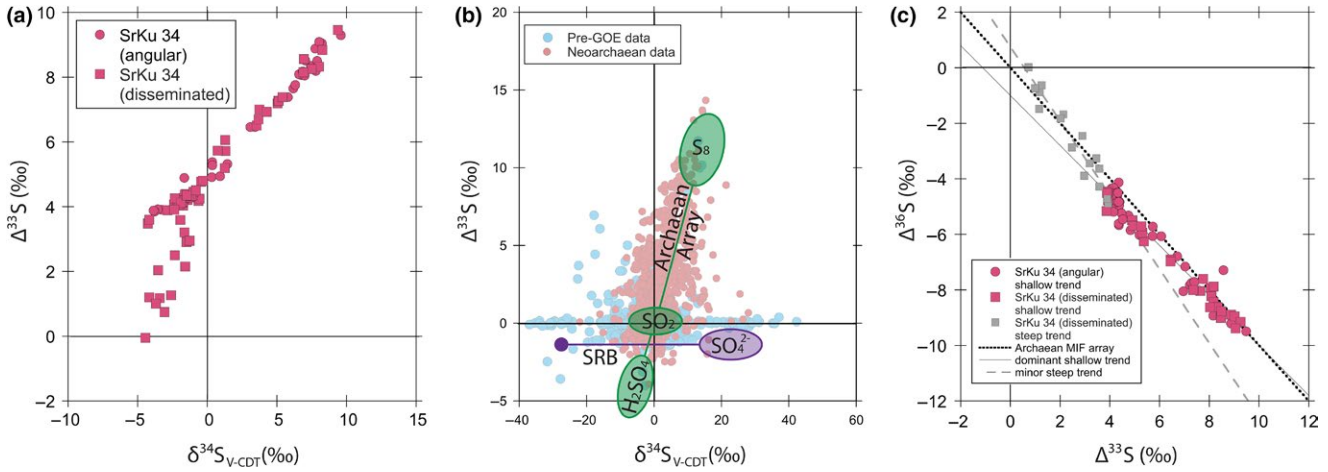

FIGURE 1 Panels a, and c illustrate new quadruple S-isotope data from analysis of the shaley limestone SrKu 34 (see Table S2 in the supporting information for data). Panel a shows a $\delta^{34}S_{V\text{-}CDT}$–$\Delta^{33}S$ plot of the new data, exhibiting two well-defined linear arrays. These arrays do not pass through the origin of the $\delta^{34}S_{V\text{-}CDT}$–$\Delta^{33}S$ plot, instead intercepting $\Delta^{33}S$ at a value of ca. + 5 ‰ and + 4 ‰ (see Figure 2b). The major, shallowly sloping trend (Figure 2b, m = 0.444) is picked out by both angular and disseminated pyrite morphologies while the minor, more steeply sloping trend (Figure 2b, m = 0.848) is picked out only by a small portion of the disseminated pyrite. Panel b shows compiled Neoarchaean and other pre-GOE MIF-S data, with the Neoarchaean data depicting the Archaean array. Many data points fall on an empirical linear trend in $\delta^{34}S$–$\Delta^{33}S$ ($\Delta^{33}S = 0.9 \times \delta^{34}S$; Ono et al., 2003), termed the Archaean array. This is widely interpreted to reflect formation of sulphides formed by mixing sulphur from two primary atmospheric sources carrying opposite S-MIF signals; reduced sulphur, e.g., S_8 ($\Delta^{33}S$ >0), and residual oxidised sulphur, e.g., SO_2 and/or H_2SO_4 ($\Delta^{33}S$ <0), both of which are rained out to the hydrosphere and subsequently delivered to the ocean and sediments (Farquhar et al., 2001; Ono et al., 2003). Additionally, S-species may be subject to MDF and exhibit fractionation in $\delta^{34}S$, along the SRB trend parallel to the $\delta^{34}S$ axis. Panel c shows a $\Delta^{33}S$–$\Delta^{36}S$ plot of the new Gamohaan Fm. data from SrKu 34. All of the angular SrKu 34 pyrite data, and some of the disseminated SrKu 34 pyrite data define a very strong linear trend in $\Delta^{36}S$ vs. $\Delta^{33}S$ with the typical slope of 0.9 but a negative $\Delta^{36}S$ intercept of −1, while the rest of the disseminated SrKu 34 pyrite data define a linear regression line $\Delta^{36}S$ vs. $\Delta^{33}S$ with a steeper slope (−1.3) and a positive $\Delta^{36}S$ intercept of 0.75. The bold black dotted line represents the Archaean MIF array (e.g., Shen, Farquhar, Masterson, Kaufman, & Buick, 2009), exhibiting the characteristic negative $\Delta^{33}S$–$\Delta^{36}S$ correlation with a slope of ca. −1, reported from Archaean sulphides

in a progressively deepening depositional environment (Fischer et al., 2009). Sample SrKu 31 is a contorted microbial mat limestone containing spheroidal pyrite grains (typically >ca. 2 mm) inferred to be of a sulphate-reducing bacterial origin (SRBO) (Kamber & Whitehouse, 2007), interpreted to have formed above the storm wave base in a shallow marine environment (Beukes, 1987).

Further up the section sample SrKu34 is located. This is a shaley limestone interbedded with microbial limestones and abiotic calcite precipitates. It is interpreted to have formed in deeper water than SrKu31, at a depth of 50–100 m, during a brief episode of drowning (Beukes, 1987). Pyrite in SrKu34 is present in a range of grain sizes from massive (ca. 1 mm) concretionary solid angular aggregates, to fine-grained (typically <ca. 20 μm) and disseminated (figure 5: Kamber & Whitehouse, 2007). Previous studies (Kamber & Whitehouse, 2007; Whitehouse, 2013) reported a range of 7.5 ‰ $\Delta^{33}S$ within a 15 × 5 mm cutting from a single 76 × 26 mm thin section of this sample. In addition, data from this single sample define a strong linear array that clearly does not pass through the origin of the $\delta^{34}S_{V\text{-}CDT}$–$\Delta^{33}S$ plot (Kamber & Whitehouse, 2007), thus strongly deviating from the "Archaean" array (Ono et al., 2003).

There is agreement that the Gamohaan Formation was deposited during subsidence of the underlying carbonate platform, eventually giving rise to the deeper water Kuruman Formation. However, opinions diverge regarding the nature of the subsidence event. Beukes (1987) and Klein and Beukes (1989) envisaged whole-sale drowning of the platform, whereas Altermann and Siegfried (1997) and Altermann and Nelson (1998) proposed that there was significant topography across the platform, with emergent palaeo-highs in amongst poorly connected shallow sub-basins. There is clear evidence that the predominant shallow marine limestone deposition was interrupted by shale and, more rarely, volcanic tuff emplacement (e.g., Altermann & Siegfried, 1997). Hälbich (1992) commented on the facies variability along strike of the Gamohaan Formation and the frequent intermittent return of fine-grained clastic sedimentation, implying a relatively proximal source of continental sediment. In their Palaeoproterozoic plate reconstruction of the Zimbabwe, Kaapvaal and Pilbara cratons, Zeh, Wilson, and Ovtcharova (2016) proposed the existence of a "Hamersley" arc-retro arc system to the west of the study area as the source of the tuff horizons and shales, found to be associated with carbonates in the Campbellrand Subgroup. As will become apparent, we attribute special importance to the position of shale beds and tuffs for the interpretation of S-isotope systematics.

3 | METHODS

Sulphur isotopes (^{32}S, ^{33}S, ^{34}S and ^{36}S) were analysed using a CAMECA IMS1280 ion microprobe at NordSIM, Swedish Museum of Natural

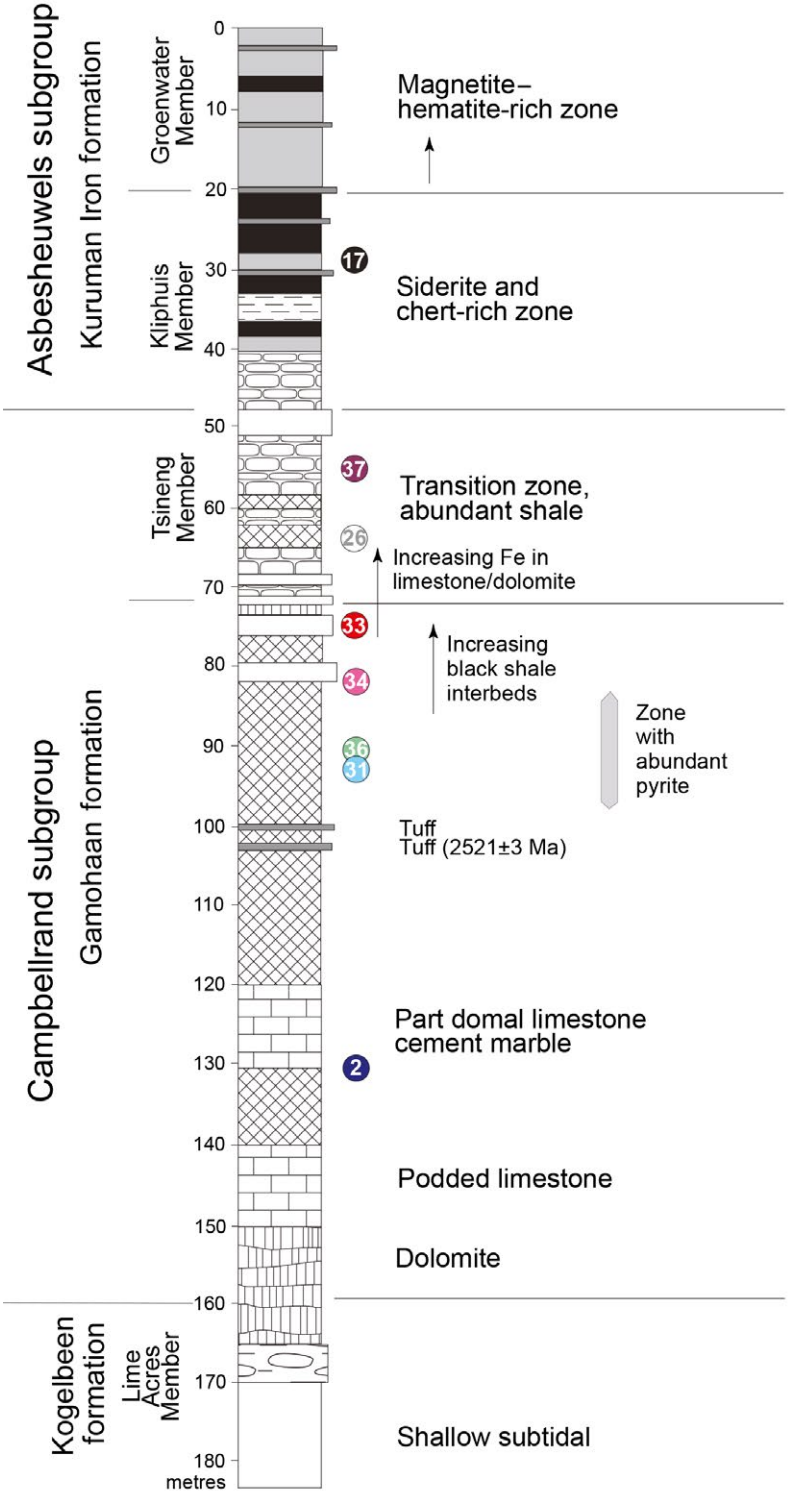
Asbesheuwels subgroup
Kuruman Iron formation
Groenwater Member
Kliphuis Member
Campbellrand subgroup
Gamohaan formation
Tsineng Member
Kogelbeen formation
Lime Acres Member
0
10
20
30
40
50
60
70
80
90
100
110
120
130
140
150
160
170
180
metres
17
37
26
33
34
36
31
2
Magnetite–hematite-rich zone
Siderite and chert-rich zone
Transition zone, abundant shale
Increasing Fe in limestone/dolomite
Increasing black shale interbeds
Zone with abundant pyrite
Tuff
Tuff (2521±3 Ma)
Part domal limestone cement marble
Podded limestone
Dolomite
Shallow subtidal
Hematite–Magnetite BIF
Magnetite–Siderite BIF
Siderite BIF
Siderite–Ankerite banded chert
Stilphomelane lutite (tuff)
Finely laminated carbonaceous limestone
Limestone with or without various stromatolites
Fenestrated limestone
Giant domal stromatolites
Chert

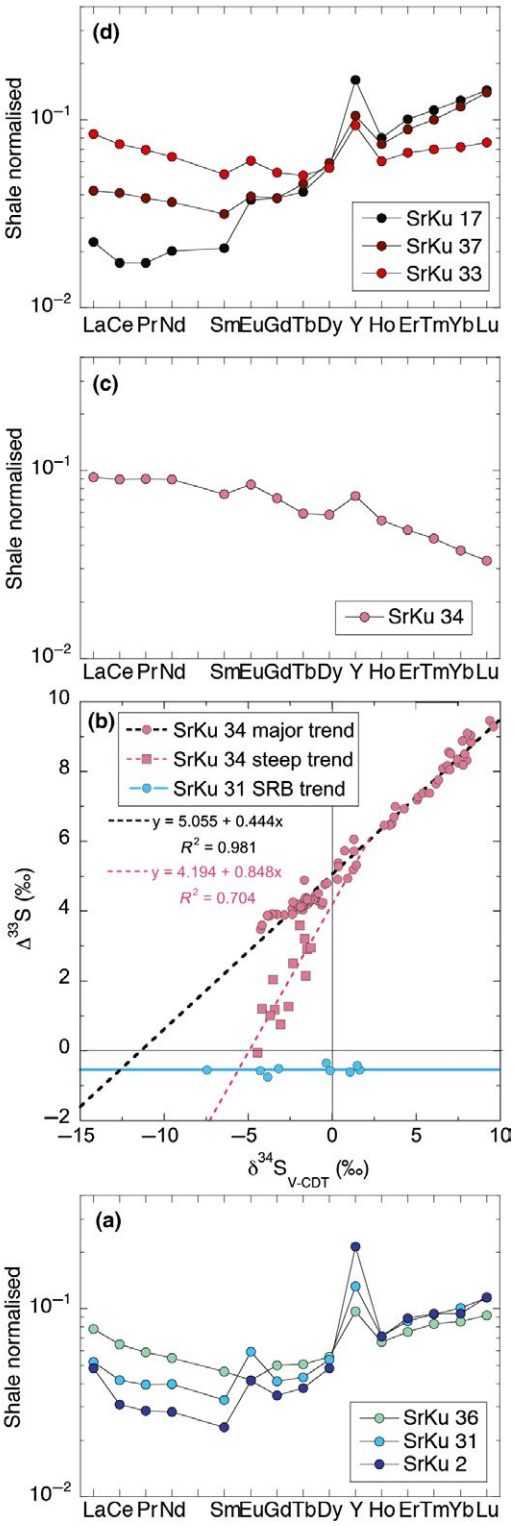
(d)
Shale normalised
SrKu 17
SrKu 37
SrKu 33
LaCe PrNd SmEuGdTbDy Y Ho ErTmYbLu
(c)
SrKu 34
(b)
SrKu 34 major trend
SrKu 34 steep trend
SrKu 31 SRB trend
y = 5.055 + 0.444x
R² = 0.981
y = 4.194 + 0.848x
R² = 0.704
Δ33S (‰)
δ34SV-CDT (‰)
(a)
SrKu 36
SrKu 31
SrKu 2

FIGURE 2 Schematic lithostratigraphic context of the studied samples, including representative REE+Y patterns of carbonates and selected S-isotope plots. The positions of all samples discussed in text are shown relative to stratigraphic depth in the drill core. The tuff bed at 103 m depth was dated to 2521 ± 3 Ma by Sumner and Bowring (1996). Insets a, b and d show representative REE+Y diagrams (see Table S1 in the supporting information for data). The symbols are colour-coded from dark blue (deepest in core) grading to pink (middle) and further to dark red and black (shallowest in core). The shape of the patterns shows a coherent trend, starting with steeply positive slopes and typical marine features (e.g., SrKu 2). Up core, the LREE start to increase in abundance and the patterns flatten out (inset a), exemplified by calcareous shale sample SrKu34 (inset c). Further up the core, the trend is reversed and patterns become steeper again with more prominent marine features, as shown, for example, by sample SrKu 17 (inset d). The data were first normalised with local shale SrKu 32 (see supporting information Table S1) followed by vertical transposition to a constant sum of normalised values of 1 to aid visual comparison. Inset b shows a $\delta^{34}S_{V\text{-}CDT}$–$\Delta^{33}S$ plot of the newly reported SrKu 34 S-isotope data, along with previously reported (Kamber & Whitehouse, 2007) data for SrKu 31. The spheroidal pyrites of SrKu 31 exhibit consistently negative MIF-S, with consistent $\Delta^{33}S$ values of ca. −0.54 ‰ and variable $\delta^{34}S$ values, indicative of a sulphate-reducing bacterial origin (SRBO)

History, Stockholm. Analytical settings are described briefly below, and closely follow those reported in Kamber and Whitehouse (2007), and Whitehouse (2013). Sulphur was sputtered using a $^{133}Cs^{+}$ primary beam with 20 kV incident energy (10 kV primary, −10 kV secondary) and a primary beam current of ~1.5 nA, producing secondary ions from a slightly elliptical area ~10 μm in diameter (long axis). A normal-incidence low-energy electron gun was used for charge compensation. Analyses were performed in automated sequences, with each analysis comprising a 70-s pre-sputter to remove the gold coating of the sample mount over a rastered 15 × 15 μm area, the secondary beam being centred in the field aperture to correct for small variations in surface relief, and data acquisition in 24 4-s integration cycles. The magnetic field was locked at the beginning of the session using an NMR field sensor. Secondary ion signals of all four S isotopes were detected simultaneously using three Faraday detectors (for ^{32}S, ^{33}S and ^{34}S) and an ion counting electron multiplier (^{36}S), with a mass resolution appropriate to resolve ^{33}S from $^{32}S^{1}H$ (ca. 4860 M/ΔM).

Data were normalised for instrumental mass fractionation using matrix-matched standards mounted together with the sample mount and analysed after every seventh sample. The standards were Ruttan pyrite and Balmat pyrite, with conventionally determined values of +1.2 ‰ and + 15.1 ‰, respectively (Crowe & Vaughan, 1996). However, recent detailed re-evaluation (Whitehouse, 2013) of the pyrite standards has resulted in slightly higher recommended values (+ 1.41 ‰ for Ruttan and + 16.52 ‰ for Balmat, reported in Cabral et al., 2013), which were used for normalisation in this study. External precision (standard deviation) based on the observed $\delta^{3x}S$ values from the primary standard (Ruttan) were propagated onto the reported $\delta^{3x}S$ values in quadrature with the run errors, while the external precision on $\Delta^{3x}S$ values are the maximum of the external based on $\Delta^{3x}S$ values from both non-MIF standards or the run $\delta^{3x}S$ value. The typical precision of $\delta^{34}S$, $\Delta^{33}S$ and $\Delta^{36}S$ values, after propagating the within-run and external uncertainties from standard measurements, were ±0.09 ‰, ±0.04 ‰ and ±0.26 ‰, respectively. All results are reported with respect to the Vienna-Canyon Diablo troilite (V-CDT) meteorite standard (Ding et al., 2001). In addition to these standards, a MIF-positive pyrite from the early Archaean banded iron formation (BIF) in the Isua Greenstone Belt, which previously yielded $\Delta^{33}S$ of + 3.18 ± 0.05 ‰, and $\Delta^{36}S$ of −2.20 ± 0.21 ‰ (95% confidence interval) by SIMS (Whitehouse, 2013), was analysed seven times during this study. The seven analyses yielded an average $\Delta^{33}S$ of + 3.12 ± 0.11 ‰ (±1 σ), and $\Delta^{36}S$ of −2.44 ± 0.25 ‰ (±1 σ), confirming the reproducibility of the SIMS method.

New rare earth element (REE) data are reported for a few samples bracketing the pyrite-bearing limestones and the shaley limestone. These were obtained with routine solution quadrupole ICP-MS method after preferential digestion of the carbonate fraction in 5% triple-distilled HNO_3 (Kamber, Webb, & Gallagher, 2014).

In order to verify the possibility that the recorded Neoarchaean MIF-S might not average the canonical terrestrial value of V-CDT, statistical analysis of compiled, previously published Neoarchaean and other pre-GOE MIF-S data were performed (Figure 3). Neoarchaean data were defined as those having been obtained from Neoarchaean rocks, that is aged between 2500 and 2800 Ma. Pre-GOE data were defined as those having been obtained from rocks aged between 2320 and 4000 Ma, excluding all Neoarchaean data. Separate analysis of three distinct lithological subdivisions was also undertaken. The supporting information gives further detail on how the lithological subdivisions were defined. The compiled data are from references assembled in Reinhard et al. (2013); see supporting information for a full list of references. For each subset of data, the sample size (n), the range of values, that is the maximum and minimum, the mean, the first quartile, the median, and the third quartiles of the data are provided.

4 | RESULTS

The new REE+Y data are reported in Table S1 of the supporting information and illustrated in stratigraphic context (Figure 2a, c, and d). The shale normalised REE+Y patterns display a coherent trend with respect to stratigraphic depth. A marine origin with an open ocean signal is indicated for the stratigraphically lowest samples (SrKu 2, SrKu 31, and SrKu 36) (Figure 2a). These samples show the well-established marine REE features, such as a positive slope (Pr/Yb <1), a positive La anomaly and a superchondritic Y/Ho ratio (see Kamber et al., 2014 for a full discussion) that were originally reported for the Gamohaan Formation by Kamber and Webb (2001). By contrast, up section, SrKu34 exhibits a relatively flat shale normalised REE+Y pattern (Figure 2c) indicative of deposition in a more restricted basin, while further up the section, the REE+Y patterns of samples from the top of the formation (SrKu 33, SrKu 37 and SrKu 17) (Figure 2d) return to those typical of more open marine conditions (Kamber et al., 2014).

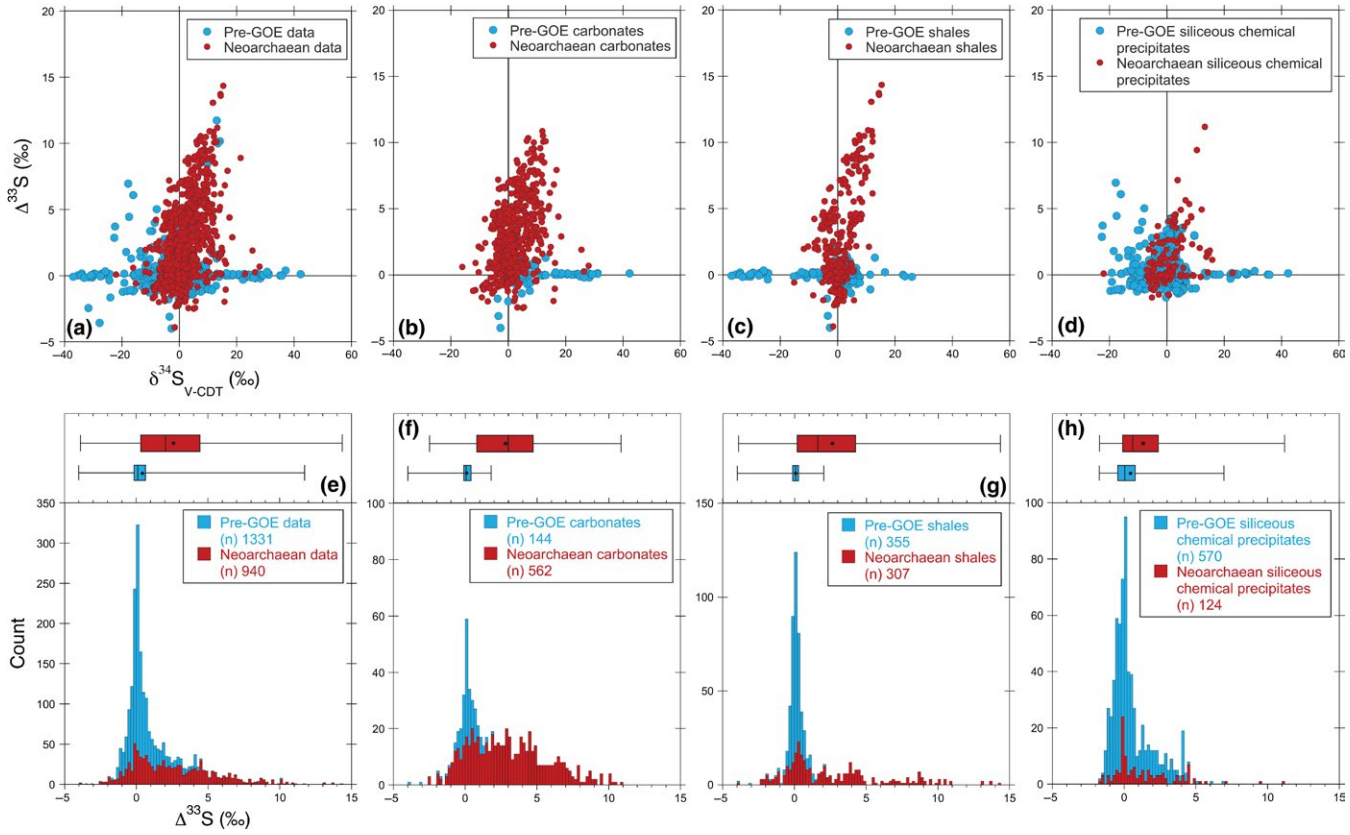

FIGURE 3 Four $\delta^{34}S_{V\text{-}CDT}$–$\Delta^{33}S$ plots of compiled, previously published MIF-S data (a), along with the data subdivided into three distinct lithological types; carbonates (b), shales (c) and siliceous chemical precipitates (d, including chert, BIF and barite). Compiled, previously published, Neoarchean MIF-S data are shown in red, while all other pre-GOE data, excluding the Neoarchaean data, are shown in blue. Panels e to h show corresponding histograms and box and whisker plots identically colour-coded. The range in magnitude of analysed $\Delta^{33}S$ values is illustrated with histograms. The histogram bin size represents 0.2 ‰ $\Delta^{33}S$, within the range of 0.06 ± 0.16 ‰ (average ±2 *SD*) of all mass dependently fractionated data from the past 2.2 Ga (Reinhard et al., 2013). In each case, the number of analyses (*n*) for both Neoarchaean and other pre-GOE data is noted. See the supporting information for a full list of references used for this compiled, previously published MIF-S database. In box and whisker plots, the whisker ends illustrate maximum and minimum values, the box illustrates the interquartile range with the median at the centre, and the mean value in each case is superimposed on the box and whisker plot as a black filled circle. See Table S3 for full details of the statistical data used for these plots

In situ secondary ion mass spectrometer quadruple S-isotope data for SrKu 34 are reported in Table S2 of the supporting information, photomicrographs of analytical sites are given in Figure S1 of the supporting information, and interested readers are referred to figure 5 of Kamber and Whitehouse (2007) for greater petrographic context. The new data confirm and extend the extreme range in MIF-S recorded in this relatively small, single sample, ranging from $\Delta^{33}S$ of 0 to + 9.5 ‰ (Figure 1a). The new data also confirm and expand the previously established linear arrays and nonzero intercept in the $\delta^{34}S_{V\text{-}CDT}$–$\Delta^{33}S$ plot (Kamber & Whitehouse, 2007; Whitehouse, 2013). There is a dominant, shallow trend (m = 0.44) and a secondary, steeper trend (m = 0.85), neither of which intersect the origin, instead intercepting $\Delta^{33}S$ at ca. + 5.06 ‰ and ca. + 4.19 ‰, respectively (Figure 2b). In detail, both the solid angular pyrite and the fine-grained disseminated pyrite from SrKu 34 define the dominant, nonzero intercept linear trend, while only a small portion of the fine-grained disseminated pyrite from SrKu 34 defines the minor, more steeply sloping, nonzero intercept linear trend (Figure 1a). Both the angular and disseminated SrKu 34 pyrite data exhibit the characteristic negative $\Delta^{33}S$–$\Delta^{36}S$ correlation with a slope of −1 (e.g., Farquhar et al., 2000), reported for many Archaean sulphides (Figure 1c). For the purpose of discussion, the newly reported S-isotope data for SrKu 34 are shown along with compiled MIF-S data for Neoarchaean and other pre-GOE sulphides (Figure 1b), and previously reported (Kamber & Whitehouse, 2007) S-isotope data for SrKu 31 (Figure 2b).

Neoarchaean and other pre-GOE MIF-S data are shown as $\delta^{34}S_{V\text{-}CDT}$–$\Delta^{33}S$ plots (Figure 3a–d), along with corresponding statistical analysis (Figure 3e–h; see Table S3 for full details of this statistical analysis). In all cases, the Neoarchaean data are seen to form an overall trend from positive $\delta^{34}S$ and $\Delta^{33}S$ towards slightly negative $\delta^{34}S$ and $\Delta^{33}S$ (Figure 3a–d), broadly delineating Ono et al.'s (2003) Archaean atmospheric array (Figure 1b). In contrast, the other pre-GOE data (i.e., all pre-GOE data excluding all Neoarchaean data) appear to cluster more tightly around the origin of the $\delta^{34}S_{V\text{-}CDT}$–$\Delta^{33}S$ plot and exhibit greater fractionation in $\delta^{34}S$ values (Figure 3a–d). In each case, the corresponding histograms with box and whisker plots illustrate the

range in magnitude of data, the maximum and minimum values, the interquartile range, the mean and the median of the compiled data (Figure 3e–h). The most important result of this analysis is that the mean $\Delta^{33}S$ value of all compiled Neoarchaean data (Figure 3e: +2.6 ‰) is significantly higher than a neutral, 0 ‰ $\Delta^{33}S_{V\text{-}CDT}$ mantle composition. This holds true for each of the Neoarchaean lithological subdivisions, with none of the lithologies showing an average 0 ‰ $\Delta^{33}S_{V\text{-}CDT}$ mantle composition (Figure 3f–h). The mean $\Delta^{33}S$ value of Neoarchaean carbonate data is furthest from a mantle composition, at a $\Delta^{33}S$ value of + 3.0 ‰ (Figure 3f), while the mean $\Delta^{33}S$ value of Neoarchaean siliceous chemical precipitates is closest to a mantle composition, albeit still well above 0 ‰ at 1.3 ‰ (Figure 3d). The absence of stronger lithological distinctions in average $\Delta^{33}S_{V\text{-}CDT}$, including between shales and carbonates, is somewhat surprising if pyrite formed via two different pathways from separate sulphur pools (Farquhar et al., 2013).

The statistical findings from the compiled Neoarchaean data contrast significantly with findings for the compiled pre-GEO database, excluding Neoarchaean data. For all lithological subdivisions, the mean $\Delta^{33}S$ value of those data is much closer to a MIF-neutral mantle composition (Figure 3e–h). The pre-GOE carbonates, excluding Neoarchaean data, have a mean $\Delta^{33}S$ value approaching 0 ‰ $\Delta^{33}S_{V\text{-}CDT}$, at 0.09 ‰ (Figure 3f). The pre-GOE siliceous chemical precipitates have a mean furthest from a MIF-neutral mantle composition, at 0.45 ‰ (Figure 3d). The magnitude of $\Delta^{33}S$ excursions for all compiled Neoarchaean data encompasses a wider range of values ($\Delta^{33}S$ from −3.9 ‰ to 14.4 ‰) than the rest of the pre-GOE data ($\Delta^{33}S$ from −4 ‰ to 11.7 ‰) (Figure 3e). Furthermore, in all cases the compiled, previously published Neoarchaean data are asymmetrical about 0 ‰, with a clear bias towards positive $\Delta^{33}S$ values (Figure 3e–h).

4.1 | The 20th-century atmospheric lead analogy

Before discussing the new data and the statistical analysis, we draw attention to the Archaean seawater sulphur concentrations (inferred to be very low) and, as such, the limitations of using modern oceanic sulphur systematics as a key to the past. Instead we propose that the 20th-century atmospheric lead event may be a better analogue for the Archaean sulphur cycle.

In the absence of oxidative weathering of terrestrial sulphides, the global pre-GOE sulphur cycle was radically different from the present situation (Fike et al., 2015; Habicht et al., 2002). To appreciate the magnitude of the difference, readers are reminded that sulphate is the second most abundant anion after chloride in the modern ocean at concentrations of 28,000 μM (Ohmoto & Felder, 1987), whereas pre-GOE seawater sulphate concentration was very low. Available estimates range from <1% (Zhelezinskaia et al., 2014) to <0.01% (Crowe et al., 2014) of that of modern sea water. Such low sulphate concentrations translate into a very short oceanic sulphur residence time, estimated at 10^3 to 10^4 years (Crowe et al., 2014). If estimates for a 10^3 years oceanic sulphur residence time are correct, these residence times are shorter than the modern day ocean mixing time, implying that the Archaean ocean was quite poorly mixed with respect to sulphur. Even if the oceanic sulphur residence time was >10^3 years, it is still possible that the mixing time of the Achaean ocean was longer owing to factors such as the smaller continental mass at that time (Collerson & Kamber, 1999), possible lack of polar ice caps and different ocean floor topography (e.g., Galer & Mezger, 1998).

In a situation where the ocean harbours a very large dissolved non-MIF sulphate inventory, it becomes impossible to transmit an atmospheric MIF-S signal into the sedimentary record. This can be illustrated with data from sulphur retrieved from modern ice caps. Unlike the ocean, present-day polar ice caps have very low sulphur concentrations (Minikin et al., 1998; Wagenbach et al., 1998) and, akin to the pre-GOE ocean, do not obtain sulphur from sulphide weathering on land. This allows for preservation of MIF-S anomalies associated with large, stratospheric volcanic eruptions (including from low latitudes) in polar ice even under the modern oxic atmosphere (e.g., Mt. Pinatubo, June 15, 1991: Baroni, Thiemens, Delmas, & Savarino, 2007; Savarino, Romero, Cole-Dai, Bekki, & Thiemens, 2003). Naturally, the extent of MIF-S measured in polar ice cores ($\Delta^{33}S$: −0.5 to + 0.7 ‰; Ono et al., 2003) is much smaller than that observed in pre-GOE sediments ($\Delta^{33}S$: −2.5 to + 12.5 ‰; Reinhard et al., 2013), because stratospheric MIF-S that may actually have reached the extreme values recorded in Archaean rocks (Baroni et al., 2007) is heavily diluted with atmospheric sulphur that shows only mass-dependent fractionation (MDF-S). The polar ice cap data thus show the limitations of using the modern oceanic sulphur systematics as a key to the past. Rather, a more useful modern analogue for the ancient sulphur cycle can come from an element that has a very short residence time in the ocean and whose main pathway to the ocean is via the atmosphere and not through the dissolved load of rivers or hydrothermal venting. Here we argue that a well-studied example of this situation is the anthropogenically dominated lead cycle of the 19th and 20th centuries.

Lead has a very low natural concentration in sea water, due in part to its high particle reactivity (Schaule & Patterson, 1981), resulting in very short oceanic residence time (2–100 years: Chow & Patterson, 1962; Bacon, Spencer, & Brewer, 1976; Nozaki, Thomson, & Turekian, 1976; Nozaki & Tsunogai, 1976). Before industrialisation, the various ocean basins had their individual, unique Pb-isotope signatures. These can, for example, be reconstructed from analysis of pre-anthropogenic hydrogenous sediments, such as ferromanganese deposits (e.g., Abouchami & Goldstein, 1995). From the distribution of the isotope values and their temporal evolution, it is possible to reconstruct aspects of the ocean circulation over the past 100 Ma or so (e.g., Ling et al., 1997) and riverine as well as volcanic aerosol input into the ocean basins (e.g., Chen, Ling, Hu, Frank, & Jiang, 2013; Van De Flierdt et al., 2003). Thus, prior to industrial pollution, local riverine and atmospheric isotope signals were transmitted to sediments on the ocean floor, yielding provincial patterns (Von Blanckenburg, O'Nions, & Heinz, 1996).

In the early 19th century, local industrial lead signals developed in response to coal burning (e.g., Arnaud et al., 2004) before large-scale mining and lead smelting and refining resulted in dominant point sources of atmospheric lead. For example, release of lead from the giant Pb-Zn-Ag deposit of Broken Hill (New South Wales) can

be quantitatively reconstructed thousands of km downwind in peat and lake sediment cores (e.g., Marx, Kamber, Mcgowan, & Zawadzki, 2010). With the advent of industrialisation and particularly with the use of tetraethyl lead as an anti-knock agent in petrol, the natural atmospheric-oceanic lead cycle became completely transformed. The addition of tetraethyl lead to petrol increased from the early 20th century to a peak in 1970, after which international bans led to the near-complete phasing out towards the end of the 20th century. Due to the fact that tetraethyl lead was largely sourced from only a few very large mines and widely distributed, hemispheric differences in the atmospheric Pb-isotope compositions were created and transposed into the oceans and eventually into coeval sediments (e.g., Patterson, 1965; Wu & Boyle, 1997). These industrial signals completely overwhelmed the pre-anthropogenic Pb-isotope provinciality but since the phase-out, more regional atmospheric pollution patterns have again become apparent (e.g., Bollhöfer & Rosman, 2002). There are thus many similarities between the industrial lead cycle and the Archaean sulphur cycles:

i) the oceanic inventories of both elements are/were low;
ii) both elements have/had short oceanic residence times;
iii) the main oceanic input was atmospheric raindown;
iv) individual giant point sources (explosive large-scale volcanic eruptions in the case of sulphur, and giant smelters in the case of lead) could at least temporally dominate atmospheric input and be transported thousands of km down-wind.

By analogy with the findings from the inadvertent industrial lead experiment, it can thus be hypothesised that in the Neoarchaean, the above factors combined permitted the effective transmission and preservation of localised MIF-S signals and that seawater sulphate and its isotopic composition were extremely sensitive to perturbations in the global sulphur cycle, particularly to large volcanic eruptions that released high quantities of sulphur.

5 | DISCUSSION

We initially address the significance and possible origin of the observed nonzero intercept $\delta^{34}S_{V\text{-}CDT}$–$\Delta^{33}S$ data array. Next we discuss the apparent temporal variation in the extent of MIF-S throughout the Archaean before concluding on the origin of the Neoarchaean bias towards positive $\Delta^{33}S$.

5.1 | The significance of the nonzero $\Delta^{33}S$–$\delta^{34}S$ intercept

Kamber and Whitehouse (2007) proposed that the main nonzero intercept $\delta^{34}S_{V\text{-}CDT}$–$\Delta^{33}S$ data array shown by sample SrKu34 could indicate diagenetic mixing of unrelated sulphur sources in the sediment environment. More specifically, recycled sulphur from basinal brines (e.g., from stratigraphically lower samples similar to SrKu31, which contained SRBO spheroidal pyrite) could have mixed with originally elemental sulphur from the water column. The geological context for this idea, from REE+Y data (Figure 2) and petrographic analysis (Kamber & Whitehouse, 2007), is that SrKu31 was deposited in open ocean, shallow water (Figure 2a) incorporating SRBO pyrite largely plotting in the bottom left quadrant of the $\delta^{34}S_{V\text{-}CDT}$–$\Delta^{33}S$ plot, with consistently negative $\Delta^{33}S$ values, ca. −0.54 ‰, and an isotopic gradient in $\delta^{34}S$ from ca. −8 to + 2 ‰ (Figure 2b). Subsequently, the basin became restricted and the carbonate platform was slightly drowned as SrKu34 was deposited in deeper water in a temporarily restricted basin (Figure 2c), while simultaneously burying the sediment below, that is strata like the host of SrKu31. Basinal fluids then potentially dissolved pyrites from sediment such as SrKu31, transporting its S-isotope signature to the sediment–water interface where it was mixed with S in the water column. Here SrKu34 pyrite grew by incorporating sulphur from these two distinct sulphur sources. The nonzero intercept array obtained from SrKu34 may thus imply a hybrid sulphur source, leading to a mixing line between sulphur with an isotopic signal similar to SrKu31 SRBO sulphate from the bottom left quadrant of the $\delta^{34}S_{V\text{-}CDT}$–$\Delta^{33}S$ plot, and water column (originally S_8) from the top right quadrant of the $\delta^{34}S_{V\text{-}CDT}$–$\Delta^{33}S$ plot (Figure 2b). Additionally, stable isotope fractionation may have altered the composition of the mobilised SRBO sulphate. The SrKu34 array is currently the best defined, but other studies have also found striking linear trends with significant nonzero intercepts. Philippot, Van Zuilen, and Rollion-Bard (2012) reported the discovery of a possible evolved volcanic sulphur source plotting in the upper left quadrant of the $\Delta^{33}S$–$\delta^{34}S$ plot. Mixing of such sulphur with remobilised sulphur from samples plotting on the reference Archaean array (Figure 1b) could also lead to linear trends similar to those observed in SrKu34. However, we believe that the extreme compositions reported by Philippot et al. (2012) for the "felsic ash data" need to first be replicated in further studies before they could be used to support our hypothesis.

Regardless, with both of these interpretations, the nonzero intercept of the array has no atmospheric significance. Both explanations require basinal fluids to have dissolved pyrite and transferred its S-isotope signature upwards and/or downwards stratigraphically. This was unlikely to have occurred via pyrite oxidation and transport of S as sulphate because of the lack of petrographic evidence for oxidation and dissolution of sulphides. Namely, very delicate microbial kerogen is preserved in exquisite detail in the limestones below the host of SrKu34 (e.g., Kamber et al., 2014; Sumner, 1997) and many of these limestones contain intricately distributed micron-scale pyrite grains with no evidence for dissolution. Furthermore, the pyrite chemistry itself (Gallagher et al., 2015) as well as the REE systematics of the hosting limestones (e.g., Kamber et al., 2014) argues strongly in favour of reducing conditions during the Gamohaan Fm.'s deposition and diagenesis.

Williford et al. (2016) also reported $\delta^{34}S_{V\text{-}CDT}$–$\Delta^{33}S$ trends with nonzero intercepts from the Neoarchaean Mount Rae Shale, the Jeerinah Formation and the Wittenoom Formation. Intercepts were found at different $\Delta^{33}S$, ranging from ~ +2 to ca. ~ +7. According to Williford et al. (2016 p.122), "the mechanisms behind these various positive intercepts were difficult to understand in the depositional

context" but the overall positive $\Delta^{33}S$ likely indicated preferential transfer of S^0 relative to SO_4^{2-} into sediment. Although the possibility of preferential transfer of the positive MIF ^{33}S via S^0 remains a viable explanation for nonzero intercepts, it does not also explain the bias towards generally positive $\Delta^{33}S$ for all analysed Neoarchaean sedimentary pyrite.

Farquhar et al. (2013) proposed that linear arrays in $\delta^{34}S_{V\text{-}CDT}$–$\Delta^{33}S$ could arise by mixing of sulphur derived from two co-existing S-pools, each with a separate pathway to pyrite formation. Although the ion-probe data for their own samples did not show clear nonzero intercepts, the possibility exists that the array defined by our own data could represent mixing between the two S-pools, if these pools could physically co-exist in the Archaean marine sedimentary environment. Farquhar et al. (2013, p. 17642) noted that "the main unresolved issue with this hypothesis is how the different forms of sulphur (sulphate-derived sulphide and zero valent-derived polysulphide) were supplied to the microenvironments where pyrite formation occurred." Whereas we agree that the possibility of separate pathways exists, we here develop an alternative explanation.

Our hypothesis for the nonzero intercept $\delta^{34}S_{V\text{-}CDT}$–$\Delta^{33}S$ main data array (Figure 1a) is that the array could represent the atmospheric signal from local rainout of aerosol from an arc volcano eruption, for example in the adjacent "Hamersley" arc-retro arc system (Zeh et al., 2016). We note that Farquhar et al. (2013) also envisaged heterogeneous distribution of S across the globe and these authors equally attributed significance to the proximity of volcanoes. However, where our hypothesis differs is that we envisage the volcano to have emitted sulphur that did not have the canonical V-CDT bulk Earth isotope composition, but rather, recycled subducted sedimentary sulphur that had a positive mean $\Delta^{33}S$ signal (Figure 3e–h, and 4). Thus, UV photolysis proceeded to fractionate the already positive $\Delta^{33}S$ of the volcanic aerosol to even higher values (+ 9.46 ‰ Δ^{33}) in the S_8 phase, and lower the sulphate phase towards lower, but still positive values (ca. + 3.5 ‰ $\Delta^{33}S$). Thus, with respect to the original MIF-positive volcanic aerosol, the sulphate phase was MIF-negative, even if, with respect to V-CDT, it remained positive. The original MIF-positive volcanic aerosol's isotopic composition cannot be accurately established because the $\delta^{34}S$ value of the aerosol is not known. If the $\Delta^{33}S$ was already positive, UV photolysis would have fractionated it to even higher values. The slope of the main nonzero intercept array (m = 0.44, Figure 2b) is very similar to the slopes of the nonzero intercept arrays reported by Williford et al. (2016), less steep than that of the "Archaean array" (m = 0.89, Figure 1b) proposed by (Ono et al., 2003) but is much more similar than the negative slope of data reported by Philippot et al. (2012). However, if similar arrays to those reported by Philippot et al. (2012) can be reproduced in other laboratories, in the context of our model, these too may be the product of single volcanic degassing episodes. Since our model envisages an isolated volcanic emission, it is possible that the recorded slope is characteristic of UV photolysis operating at specific atmospheric height, unlike the global background sulphur whose UV photolysis reflected reactions across the entire stratospheric and atmospheric cross section. In our explanation, the secondary steeper array (m = 0.85, Figure 2b) that is recorded only by some of the disseminated pyrite could indicate resumption of background sulphate delivery from the wider basin, with the more normal lower $\Delta^{33}S$ composition. The larger, coarser grained, angular aggregates of pyrite appear to overgrow the finer, disseminated pyrite (Kamber & Whitehouse, 2007), with far greater $\delta^{34}S$ and $\Delta^{33}S$ variability exhibited by the finer, disseminated pyrite. However, greater variability possibly existed in the earlier disseminated pyrite, which formed the precursor to the later angular aggregates of pyrite, similar to the findings of Williford et al. (2016).

With respect to the $\Delta^{36}S$ vs. $\Delta^{33}S$ systematics of our samples, we note (Figure 1c) that those data points that make up the dominant shallow $\delta^{34}S$ vs. $\Delta^{33}S$ trend, define a very strong linear trend in $\Delta^{36}S$ vs. $\Delta^{33}S$ with the typical slope of 0.9 but a negative $\Delta^{36}S$ intercept of −1. By contrast, the data points that define the steeper $\delta^{34}S$ vs. $\Delta^{33}S$ trend fall on a linear regression line $\Delta^{36}S$ vs. $\Delta^{33}S$ with a steeper slope (−1.3) and a positive $\Delta^{36}S$ intercept of 0.75. This intercept is similar to the trend for sample GKF01-1102.6 m in Farquhar et al. (2013) but we note that for all their other samples, these authors forced $\Delta^{36}S$ vs. $\Delta^{33}S$ regressions through the origin. Williford et al. (2016) also found certain samples of the Mount McRae shale to define regression lines with positive $\Delta^{36}S$ intercepts. These authors interpreted the consistency of slopes of ca. 0.9 to infer relative stability of atmospheric MIF production but noted that the significance of the intercepts remained more difficult to interpret. By contrast, Zerkle, Claire, Domagal-Goldman, Farquhar, and Poulton (2012) documented strong deviations in slopes (−1.5 to −0.9), which these authors interpreted to the state and composition of the atmosphere. In our working model, the possibility exists that the deep arc-volcanic sulphur source experienced mass-dependent isotope fractionation, variably changing the $\delta^{34}S$, $\Delta^{33}S$ and $\Delta^{36}S$ ratios, which could help to explain nonzero intercepts not just in $\delta^{34}S$ vs. $\Delta^{33}S$ space but also in $\Delta^{36}S$ vs. $\Delta^{33}S$. Furthermore, volcanic emission plumes to various atmospheric heights could also result in differing isotopic pathways (i.e., affecting slopes).

We appreciate that the idea of emitting volcanic aerosols with non-V-CDT S-isotope composition is a significant departure from the current paradigm. Before justifying this proposal, we stress here again that the stratigraphic context (Figure 2) informs us that the most pyritiferous sample, exhibiting the most extreme S-fractionation with a nonzero intercept $\delta^{34}S_{V\text{-}CDT}$–$\Delta^{33}S$ data array, is in stratigraphic proximity with shale beds and tuffs. We interpret this to imply temporary basin restriction (Hälbich, Lamprecht, Altermann, & Horstmann, 1992), increasing the likelihood of trapping more isolated sulphur emissions. Thus, we do not envisage the entire atmospheric inventory to have had a non-V-CDT S-isotope composition. Rather, an isolated volcanic aerosol emission experienced UV photolysis at a specific atmospheric height and was transmitted into a local, partly restricted basin. For reference, we draw attention to the 15 June 1991 eruption of Pinatubo, whose plume travelled west to south-west, forming a layer of aerosol at heights approximately 20–25 km above sea level, with main rainout occurring across the South China Sea (Oppenheimer, Scaillet, & Martin, 2011).

It is noteworthy that distinctive volcanic ash layers occur throughout the Gamohaan Formation. The resulting tuffs are present above

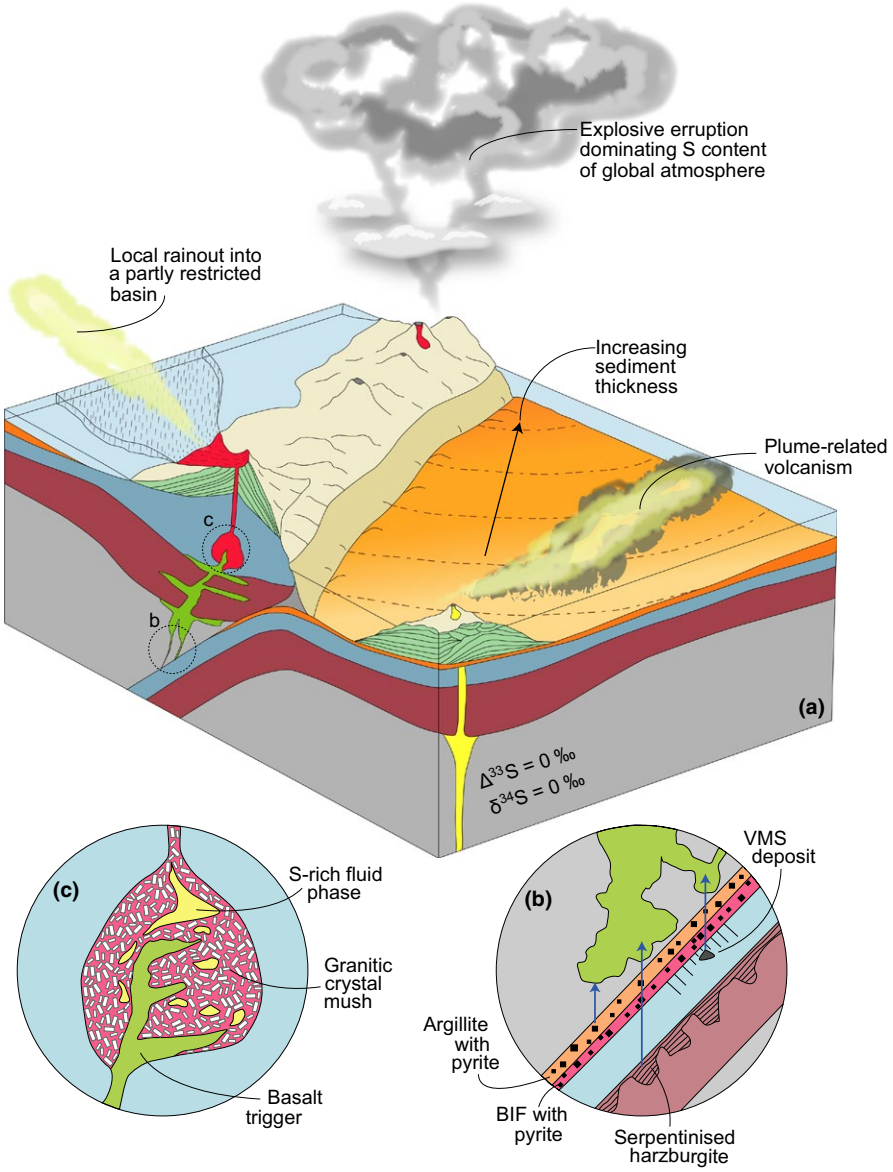

FIGURE 4 Schematic illustration of terrestrial magmatism at play during the Neoarchaean, depicting three distinct volcanogenic sources of atmospheric sulphur. The block diagram (a) depicts a newly formed, Neoarchaean subduction zone and resultant volcanic arc, in addition to a hotspot volcano, more typical of the plume-related volcanism prevalent throughout the early Archaean. The hotspot volcano quiescently degasses 0 ‰ $\Delta^{33}S_{CDT}$ mantle sulphur to the atmosphere. Subsequent atmospheric UV interaction with this mantle CDT type S imparted a MIF-S signal before incorporation into sedimentary sulphides of the oceanic crust. Once effective subduction was underway, sedimentary sulphides may have been recycled from the subducting oceanic plate into the melt source of the arc volcano, and released as anomalous nonzero $\Delta^{33}S$ MIF-S. The oceanic sediments depicted in the block diagram show a colour gradient and contours representative of thickness illustrating that oceanic crust with thicker sediment was more successful in transferring MIF-S into the subduction zone. Additionally, the transfer of sulphur is highly dependent on rock type (insert b). Potential S-sources in the subducted Archaean oceanic crust include argillite, BIFs, VMS deposits and serpentinised harzburgite (insert b). Sulphur from VMS deposits is difficult to mobilise (Ulrich, Long, Kamber, & Whitehouse, 2011) and not likely a significant contributor to the subduction zone melt source, while the subduction of lithospheric mantle, that is serpentinised harzburgite, is a potential source when undergoing devolatisation and expulsion of sulphur (Evans, 2012). Only 10% of sedimentary sulphur from mud is estimated to make it to the subduction zone melt source (Evans, Tomkins, Cliff, & Fiorentini, 2014), analogous to Archaean argillite. Liberation of sulphur from BIF sulphides (Thurston et al., 2012), BIF may have had the largest potential for preferential release of S in the subduction zone. The diagram also highlights how explosivity of eruptions determines the potential for production of a global S-signal. Basaltic recharge into an evolved magma reservoir (Pallister, Hoblitt, Meeker, Knight, & Siems, 1996; Pallister, Hoblitt, & Reyes, 1992), can separate a SO_2 rich aqueous fluid (liquid and gas) phase and trigger an eruption (insert c) releasing several million tonnes of SO_2 into the atmosphere (e.g., Bluth, Doiron, Schnetzler, Krueger, & Walter, 1992; Daag et al., 1996). Also shown is local rainout from a lesser eruptions into a restricted basin that may have facilitated preservation of an isolated S-signal

and below SrKu34 (Figure 2) and these have been used for U/Pb zircon geochronology (e.g., Sumner & Bowring, 1996), providing strong evidence for relatively proximal, explosive volcanism from evolved magmas (that permitted crystallisation of zircon), possibly in the adjacent "Hamersley" arc-retro arc system (Zeh et al., 2016). Finally, there is evidence that the Gamohaan basin was sulphate-limited; not only is the range in $\delta^{34}S$ limited (Domagal-Goldman, Kasting, Johnston, & Farquhar, 2008; Guo et al., 2009; Papineau et al., 2005; Whitehouse, 2013) but several Gamohaan Formation spheroidal pyrites also preserve $\delta^{34}S$ isotopic gradients as a function of their spherical segment radius, suggesting a limit on sulphate availability during BSR (Gallagher et al., 2015; Kamber & Whitehouse, 2007). Thus, sulphur fallout could easily overwhelm the ambient isotopic signal.

5.2 | The significance of the wide range in Neoarchaean $\Delta^{33}S$

The implicit assumption from global compilations of the $\Delta^{33}S$ MIF record is that the maxima and minima recorded correspond to the least hybridised and thus purest end-member isotope compositions of sulphur species formed by prevailing UV photolysis. Consequently, the very large Neoarchaean spread in $\Delta^{33}S$ is argued to have global atmospheric significance and is seen as a global phenomenon that persisted for some 150–200 Ma. According to this interpretation, the sulphur cycle can be modelled with a mass conservation approach. Here we propose to consider the implications of the possibility that the sedimentary record preserves local signals and that maxima and minima do not represent global end members.

In this alternative explanation, the extent of UV photolysis-induced MIF-S fractionation occurring in the atmosphere could have remained relatively unchanged throughout the Archaean. The greater extent of Neoarchaean observed $\Delta^{33}S$ was instead caused by two evolutions. Firstly, consensus is beginning to emerge that the onset of Wilson-type plate tectonics was in the lead-up to the Neoarchaean (at ca. 3 Ga; Shirey & Richardson, 2011). The associated advent of subduction of sediment, from which sulphur with pre-existing MIF signals was recycled into arc magmas and eventually released as volcanic aerosols into the atmosphere (Figure 4), provides a rationale for the emission of Neoarchaean volcanic aerosol plumes of non-V-CDT average composition. Depending on the combination of type of seafloor subducted and type of devolatilisation reaction in an arc segment, it appears feasible that locally, higher or lower $\Delta^{33}S$ than V-CDT sulphur aerosol could have been emitted by volcanoes. Once the sulphur experienced the same extent of UV photolysis-induced MIF-S, lower and higher extreme $\Delta^{33}S$ were produced. This scenario is discussed in greater detail in the final section.

Secondly, the establishment of the first platformal carbonate factories occurred at ca. 2.65 Ga (Fedo & Eriksson, 1995). Evidence for such carbonate factories is found both on the Kaapvaal Craton (i.e., the Gamohaan Fm.) and on the Pilbara Craton (i.e., the Carawine dolomite) and also on the São Francisco Craton (i.e., the Batatal Fm.). These sedimentary environments were characterised by a proliferation of microbial life, preserved as an unprecedented diversity of stromatolites (e.g., Hofmann, 2000; Schopf, Kudryavtsev, Czaja, & Tripathi, 2007). On these shallow, high organic productivity platforms, sulphate concentrations may have been very low. They also provided an environment in which local sub-basins evidently formed (e.g., Hälbich et al., 1992). The importance of these is that local aerosol signals from single volcanic events could quickly be transmitted into the sediment of such sub-basins, as exemplified by sample SrKu34. These settings thus provided an ideal environment to rapidly transfer discrete aerosol signals without dilution with the more global marine background signal. It may be significant that when omitting samples from the Kaapvaal and Pilbara cratons, the remaining Neoarchaean data show much less extreme $\Delta^{33}S$ values ($\Delta^{33}S$: −3 ‰ to + 2.12 ‰). Because at the time of sediment deposition, these two cratons were likely adjacent parts of an originally larger craton (i.e., Vaalbara; Nelson, Trendall, & Altermann, 1999; Zegers, De Wit, Dann, & White, 1998), the evidence for global extreme $\Delta^{33}S$ actually only comes from one large platform and its sub-basins.

The discussion of the temporal evolution of the extent of $\Delta^{33}S$ has attributed most significance to the range in positive values. Here we draw attention to the negative values and to the ability of our new hypothesis to explain variations in these. We note that three broadly contemporary carbonate-hosted Neoarchaean datasets show distinctive negative $\Delta^{33}S$ values. The most negative $\Delta^{33}S$ values are found in the Batatal Fm. which preserves $\Delta^{33}S$ values as low as −3 ‰ (Zhelezinskaia et al., 2014). By contrast, the Carawine dolomite preserves negative $\Delta^{33}S$ extremes of −2.5 ‰ (Ono et al., 2003), while the contemporaneous Gamohaan Fm. preserves negative $\Delta^{33}S$ extremes of −0.9 ‰ (Kamber & Whitehouse, 2007). Our hypothesis could provide an explanation for why different magnitudes of negative MIF-S were preserved, namely the most negative minimum $\Delta^{33}S$ values would form from aerosol plumes that on average, already had negative MIF relative to V-CDT, whereas only slightly negative minimum MIF could imply local average sulphur with mildly V-CDT-positive composition. Indeed, it is possible that MIF-neutral S could represent negatively MIF fractionated sulphur from local positive aerosols that, on average, were already moderately V-CDT positive. In summary, the large MIF-S excursions in global Neoarchaean $\Delta^{33}S$ compilations could be superpositions of local signals, which reflect atmospheric processing of individual volcanic eruptions.

5.3 | The Neoarchaean positive $\Delta^{33}S$ bias

Because the predominant source of seawater sulphate in the Archaean was volcanogenic, the evolving nature of terrestrial magmatism may have strongly influenced the quantity, species and isotope composition of sulphur emitted into the Archaean atmosphere. The possibility of recycling of sedimentary sulphides at subduction zones is of paramount importance. In this regard, it is important that anomalous $\Delta^{33}S$ sulphide inclusions in 2.9 Ga diamonds have been interpreted as direct evidence for recycling of sedimentary sulphur (Farquhar et al., 2002). Diamond sulphide inclusions exhibit a major compositional change at 3 Ga, when eclogite inclusions resembling metamorphosed basaltic crust become more prevalent. This has been interpreted as

the capture of eclogite via subduction (Shirey & Richardson, 2011) and that Wilson cycle plate tectonics were in operation from 2.9 to 3.0 Ga onwards (Dhuime, Hawkesworth, Cawood, & Storey, 2012)

The subduction of sediment to sufficient depth for capture by arc magmas alone is not sufficient to support the notion that individual arc eruptions could have emitted sulphur of non-V-CDT composition. Modern subduction zone studies offer some insight but like the modern marine analogue, the major issue is that modern subduction zones contain a lot more sulphide than would have been possible in the Archaean, because of the much lower sulphate content of Archaean sea water. The Archaean seafloor was also likely of a very different composition than at present. Nonetheless, modern studies show that arc magmas have $\delta^{34}S$ heavier than mantle, implying that slab-derived sediments are significant contributors to the sulphur flux in subduction zone volcanoes (De Hoog, Taylor, & Van Bergen, 2001; Métrich, Schiano, Clocchiatti, & Maury, 1999).

A possibly very important insight from modern arcs is that only a small proportion of the total subducted sulphur is actually recycled at volcanoes. For example, Evans (2012) estimated that <20% of sulphur subducted in sediments, altered oceanic crust and serpentinised lithospheric mantle is recycled. Jégo and Dasgupta (2013) estimated that 15%–30% of the subducted sulphur is returned to surface reservoirs by arc processes. When an aqueous sulphur-rich fluid (liquid and gas) phase develops, volcanic arc magmas can form in the same subduction zone tectonic setting as porphyry-copper systems (Imai, Listanco, & Fujii, 1993). Thus, arc volcanoes emitting high quantities of sulphur can be viewed as failed potential porphyry-copper deposits (Pasteris, 1996) meaning that surface reservoirs also include sulphur that did not make it into the atmosphere. Regardless, consensus exists that today, the much larger portion of subducted sulphur is apparently transported to the mantle at depths of >150 km (Evans & Powell, 2015). This evidence for non-quantitative recycling of sulphur opens the possibility for preferential transfer of sulphur with particular isotope compositions to arc magmas. Thus, the recycled sulphur may not have had "average sedimentary" isotope composition.

In modern subduction zones, the transfer of sulphur from the slab with fluids is dependent on metamorphic grade. The most efficient transfer of sulphur from sulphides apparently occurs at eclogite facies (Giacometti et al., 2014). Although no agreement exists about the thermal structure of Archaean subduction zones, melting of eclogite facies metabasalt is widely discussed in the literature as a means of producing tonalite–trondhjemite–granodiorite magmas that show evidence of arc-type geochemistry (e.g., Kamber, Collerson, Moorbath, & Whitehouse, 2003). Thus, transfer of sulphur from the igneous portion of slabs may have been different in the Archaean.

The largest difference between Archaean and post-1.8 Ga ocean floor concerns the nature of its sediment cover. In a comprehensive study of modern trenches, Plank and Langmuir (1998) showed that the weighed average composition of subducting sediment has a relatively constant composition (e.g., SiO_2 = 58.6 ± 2.5 wt%; FeO = 5.2 ± 0.4 wt%) and that the terrigenous component far outweighs the biogenic, hydrothermal and hydrogenous components. Although no fossil Archaean trenches are preserved, there is strong evidence that the predominant non-platformal sediments were of hydrogenous nature (chert and BIF; Figure 4b). Indeed, in juvenile greenstone belts, volcanic deposits are often separated by Algoma-type BIFs, cherts and minor argillites, which collectively could represent long intervals of low clastic sedimentation rate (e.g., Thurston, Ayer, Goutier, & Hamilton, 2008). Of these sedimentary rocks, BIF could have played a key role in releasing sulphur to the *supra*-subduction zone mantle. Firstly, because of its simple chemical composition dominated by FeO and SiO_2, the resulting metamorphic mineral parageneses are also constrained to very few minerals (e.g., Mloszewska et al., 2012) with limited reaction potential with sulphides or sulphates. Secondly, there is strong evidence for secondary mobility of BIF-hosted sulphides (Thurston et al., 2012) suggesting potential for preferential sulphur release from BIFs in subduction zones. Thurston et al. (2012) reported 2704- to 2734-Ma-old BIF-related pyrite nodules with $\Delta^{33}S$ extremes of−1.5 ‰ to +4.1‰. Furthermore, the findings of our statistical analysis of the compiled pre-GEO S-isotope database show that for all lithological subdivisions, the Neoarchaean data are asymmetrical about 0 ‰, with a clear bias towards positive $\Delta^{33}S$ values (Figure 3e–h). Because the Archaean $\Delta^{33}S$–$\delta^{34}S$ array shows greater absolute variability in positive $\Delta^{33}S$ than in negative $\Delta^{33}S$, the dataset may be biased as there may be a tendency to obtain a larger number of data points from the positive $\Delta^{33}S$ samples in the hope of finding the maximum positive $\Delta^{33}S$ value. Nonetheless, this possibility for bias cannot explain why the deviation from zero values is only found in the sample of Neoarchaean age. Preferential release of such nonzero $\Delta^{33}S$ sulphur into arc magma sources could thus lead to nonzero $\Delta^{33}S$ volcanic emissions.

If it is accepted that preferential transfer of non-V-CDT sulphur into Archaean arc magmas was at least theoretically feasible, the behaviour of sulphur in the evolving magma then determined whether the signal became local or hemispheric. Only highly explosive volcanic eruptions, where a separate sulphur fluid phase developed in the magma (Figure 4c) and was released as a steam plume of SO_2 into the stratosphere (e.g., the eruption of Mount Pinatubo in 1991: Pasteris, 1996), had the potential to dominate the sulphur content of the global atmosphere, at least for several years, producing a hemispheric sulphur signal. By contrast, fast rainout from lesser eruptions into a restricted basin could have facilitated preservation of the isotopic composition of a localised volcanic source (Figure 4a). In addition, variability in the location of arc volcanoes contributes to the preservation of localised S-isotope signatures because atmospheric circulation limits the dispersion of high latitude eruptions. Thus, very little aerosol of a high latitude eruption will reach the opposing hemisphere (Oppenheimer et al., 2011). The MDF-S-isotope composition of volcanically emitted sulphur can also vary with eruption style. For example, the gas phase during early open system degassing is often ^{34}S-depleted, whereas during later large eruptions there is a correspondingly ^{34}S-enriched gas phase (Mandeville et al., 2009). Subsequent UV photolysis MIF of initially ^{34}S-depleted sulphur could further shift the isotope composition of the resultant MIF array in the $\delta^{34}S_{V\text{-}CDT}$–$\Delta^{33}S$ plot. Furthermore, the sulphur concentration of volcanic gas emitted from individual modern arc volcanoes is also highly variable (Oppenheimer et al., 2011).

In summary, there are several processes that undoubtedly influenced the S-isotope composition of volcanic emissions as the Earth transitioned from a plume-dominated planet towards Wilson-style tectonics. In this context of the evolution of Archaean magmatism, the mean +2 ‰ $\Delta^{33}S$ value of pyrite from all Neoarchaean sedimentary rocks (Figure 3a–d) may imply preferential recycling of $\Delta^{33}S$-positive sulphur in subduction zones, rather than a change in photochemical reactions or evolving atmospheric composition. The absence of this bias towards positive $\Delta^{33}S$ in older sedimentary rocks would then be a tectonic consequence, namely only after initiation of Wilson-style subduction, did transfer of sulphur from slabs to arc magmas become feasible. The extent of the MIF-S signal rapidly diminished after 2.5 Ga, some 150 Ma before evidence for the GOE. There are currently too few data to accurately reconstruct the post-Archaean MIF evolution but there is wide agreement that a major change in magmatic evolution occurred at that point (Keller & Schoene, 2012). This manifests in the geochemistry of the emplaced <2.5 Ga igneous rocks and may have strongly affected volcanic degasing.

6 | CONCLUSIONS

Previous studies modelling the sulphur cycle (e.g., Canfield & Raiswell, 1999) worked from the implicit assumption that sulphur was globally mixed in the Archaean atmosphere and hydrosphere. Here we have used the 20th-century lead analogue to propose that the low concentration and short residence time of oceanic sulphur combined with its near exclusive volcanogenic source meant that the Archaean atmosphere and ocean were more likely poorly mixed with respect to sulphur. Thus, although preservation of MIF-S in Archaean sediments continues to have implications for the Archaean redox state of the global atmosphere, Archaean sedimentary rocks may preserve local MIF-S signals.

Very large explosive volcanic eruptions had potential to inject large amounts of SO_2 into the stratosphere, where it persisted for years and could dominate the atmospheric S budget. In the sedimentary record, however, even such global events will only represent miniscule layers. Ion-probe, S-isotope data are capable of resolving micron-scale variability that may be testimony to the lack of a well-mixed, long-residence time marine S-pool. At present, it is unknown over which timescales the analysed pyrites grew; however, the prospect remains that millimetre-sized pyrite could sample multiple volcanic S-raindown events. In the context of the 20th-century lead analogue, the variability of MIF-S signals in individual Archaean pyrites does not seem surprising. Furthermore, regional rainout from lesser volcanic eruptions may have had the potential to impart very local sulphur signals, particularly if they occurred over restricted basins and at latitudes away from the equator. Such volcanic perturbations are not as visible in today's ocean due to masking of the signal by the high global oceanic sulphate pool. These implications emerging from thinking of the Archaean S-cycle in terms of the lessons learnt from the 20th-century lead "experiment" are not dependent on whether volcanoes emitted S that was non-MIF-neutral.

A further more speculative implication arises if at least some volcanoes emitted recycled sedimentary sulphur that was not MIF-neutral. This possibility does not require that the bulk of subducted material had an average composition different from the $\Delta^{33}S_{V\text{-}CDT}$ because only a small proportion of subducted S is actually transferred into the magma feeding zone of arc volcanoes. Thus, if preferential transport of either $\Delta^{33}S$ positive or negative S into the arc magma feeding zone did occur, it would seem possible that some volcanoes could emit S with non-neutral MIF. Nonzero intercept $\Delta^{33}S$–$\delta^{34}S$ data arrays could then form in basins near arc volcanoes that emitted non-neutral MIF-S. Preferential transport of non-neutral MIF-S in the subduction zone could have been aided by the very different make-up of sedimentary facies (e.g., BIF, chert, paucity of carbonate) on the Archaean ocean floor, leaving S from some subducted rocks more reactive than from others.

If this speculation is accepted, it would follow that the initiation of Wilson-style plate tectonics at ca. 3 Ga had serious consequences for the global S-cycle. The transfer of sedimentary sulphur from subduction zones to the atmosphere via newly established arc volcanoes could help to explain the deviation of Neoarchaean sedimentary sulphur from the 0 ‰ $\Delta^{33}S_{V\text{-}CDT}$ mantle composition. At least temporally and locally, the sampled atmospheric sulphur could have had a different composition from average bulk Earth, and the large Neoarchaean excursions and asymmetry could be explained by superposition of local signals.

We acknowledge that the remaining unresolved issue with our hypothesis is the speculation that Archaean arc volcanoes could have emitted non-neutral MIF-S. The unresolved issue with Farquhar et al.'s (2013) separate S-pool hypothesis is that it remains unclear how the separate pathways could have remained sufficiently isolated in the micro-environments where pyrite formed. Regardless, the plausibility of our explanation can be tested with multiple-S-isotope composition of putative Precambrian arc magmatic rocks.

ACKNOWLEDGMENTS

The Nordsim facility is operated under an agreement between the research-funding agencies of Denmark, Norway and Sweden, the Geological Survey of Finland, and the Swedish Museum of Natural History. This is Nordsim contribution 495. This analytical work was supported by a SYNTHESYS grant, SE-TAF-3395, funded by the European Community – Research Infrastructure Action under the FP7 "Capacities" Specific Programme. This research was supported by an EU FP7 Marie Curie Actions – Career Integration Grant awarded to B.S.K. which provided financial support to M.G. We thank Nick Beukes for providing samples and Claire Kamber for kindly drafting figure 4. Several reviewers helped to shape the manuscript into its intended narrative.

REFERENCES

Abouchami, W., & Goldstein, S. L. (1995). A lead isotopic study of Circum-Antarctic manganese nodules. *Geochimica et cosmochimica acta*, *59*, 1809–1820.

Altermann, W., & Nelson, D. R. (1998). Sedimentation rates, basin analysis and regional correlations of three Neoarchaean and Palaeoproterozoic sub-basins of the Kaapvaal craton as inferred from precise U-Pb

zircon ages from volcaniclastic sediments. *Sedimentary Geology*, *120*, 225–256.

Altermann, W., & Siegfried, H. P. (1997). Sedimentology and facies development of an Archaean shelf: Carbonate platform transition in the Kaapvaal Craton, as deduced from a deep borehole at Kathu, South Africa. *Journal of African Earth Sciences*, *24*, 391-IN394.

Arnaud, F., Revel-Rolland, M., Bosch, D., Winiarski, T., Desmet, M., Tribovillard, N., & Givelet, N. (2004). A 300 year history of lead contamination in northern French Alps reconstructed from distant lake sediment records. *Journal of Environmental Monitoring*, *6*, 448–456.

Bacon, M., Spencer, D., & Brewer, P. (1976). 210 Pb/226 Ra and 210 Po/210 Pb disequilibria in seawater and suspended particulate matter. *Earth and Planetary Science Letters*, *32*, 277–296.

Baroni, M., Thiemens, M. H., Delmas, R. J., & Savarino, J. (2007). Mass-independent sulfur isotopic compositions in stratospheric volcanic eruptions. *Science*, *315*, 84–87.

Bekker, A., Holland, H., Wang, P.-L., Rumble, D., Stein, H., Hannah, J., … Beukes, N. (2004). Dating the rise of atmospheric oxygen. *Nature*, *427*, 117–120.

Beukes, N. J. (1987). Facies relations, depositional environments and diagenesis in a major early Proterozoic stromatolitic carbonate platform to basinal sequence, Campbellrand Subgroup, Transvaal Supergroup, southern Africa. *Sedimentary Geology*, *54*, 1–46.

Bluth, G. J. S., Doiron, S. D., Schnetzler, C. C., Krueger, A. J., & Walter, L. S. (1992). Global tracking of the SO2 clouds from the June, 1991 Mount Pinatubo eruptions. *Geophysical Research Letters*, *19*, 151–154.

Bollhöfer, A., & Rosman, K. (2002). The temporal stability in lead isotopic signatures at selected sites in the Southern and Northern Hemispheres. *Geochimica et Cosmochimica Acta*, *66*, 1375–1386.

Cabral, R. A., Jackson, M. G., Rose-Koga, E. F., Koga, K. T., Whitehouse, M. J., Antonelli, M. A., … Hauri, E. H. (2013). Anomalous sulphur isotopes in plume lavas reveal deep mantle storage of Archaean crust. *Nature*, *496*, 490–493.

Canfield, D. E. (2004). The evolution of the Earth surface sulfur reservoir. *American Journal of Science*, *304*, 839–861.

Canfield, D. E., Habicht, K. S., & Thamdrup, B. (2000). The Archean sulfur cycle and the early history of atmospheric oxygen. *Science*, *288*, 658–661.

Canfield, D. E., & Raiswell, R. (1999). The evolution of the sulfur cycle. *American Journal of Science*, *299*, 697–723.

Chen, T. Y., Ling, H. F., Hu, R., Frank, M., & Jiang, S. Y. (2013). Lead isotope provinciality of central North Pacific Deep Water over the Cenozoic. *Geochemistry, Geophysics, Geosystems*, *14*, 1523–1537.

Cheney, E. (1996). Sequence stratigraphy and plate tectonic significance of the Transvaal succession of southern Africa and its equivalent in Western Australia. *Precambrian Research*, *79*, 3–24.

Chow, T. J., & Patterson, C. (1962). The occurrence and significance of lead isotopes in pelagic sediments. *Geochimica et Cosmochimica Acta*, *26*, 263–308.

Collerson, K. D., & Kamber, B. S. (1999). Evolution of the continents and the atmosphere inferred from Th-U-Nb systematics of the depleted mantle. *Science*, *283*, 1519–1522.

Crowe, S. A., Paris, G., Katsev, S., Jones, C., Kim, S.-T., Zerkle, A. L., … Canfield, D. E. (2014). Sulfate was a trace constituent of Archean seawater. *Science*, *346*, 735–739.

Crowe, D., & Vaughan, R. (1996). Characterization and use of isotopically homogeneous standards for in situ laser microprobe analysis of 34S/32S ratios. *American Mineralogist*, *81*, 187–193.

Daag, A. S., Tubianosa, B. S., Newhall, C. G., Tuñgol, N. M., Javier, D., Dolan, M. T., … Regalado, T. M. (1996). Monitoring sulfur dioxide emission at Mount Pinatubo. In C. G. Newhall & R. S. Punongbayan (Eds.), *Fire and Mud: Eruptions and Lahars of Mount Pinatubo, Philippines* (PP. 409–434). Quezon City: Philippine Institute of Volcanology, and Seismology and Seattle, WA: University of Washington Press.

De Hoog, J., Taylor, B., & Van Bergen, M. (2001). Sulfur isotope systematics of basaltic lavas from Indonesia: Implications for the sulfur cycle in subduction zones. *Earth and Planetary Science Letters*, *189*, 237–252.

Dhuime, B., Hawkesworth, C. J., Cawood, P. A., & Storey, C. D. (2012). A change in the geodynamics of continental growth 3 billion years ago. *Science*, *335*, 1334–1336.

Ding, T., Valkiers, S., Kipphardt, H., De Bievre, P., Taylor, P., Gonfiantini, R., & Krouse, R. (2001). Calibrated sulfur isotope abundance ratios of three IAEA sulfur isotope reference materials and V-CDT with a reassessment of the atomic weight of sulfur. *Geochimica et Cosmochimica Acta*, *65*, 2433–2437.

Domagal-Goldman, S. D., Kasting, J. F., Johnston, D. T., & Farquhar, J. (2008). Organic haze, glaciations and multiple sulfur isotopes in the Mid-Archean Era. *Earth and Planetary Science Letters*, *269*, 29–40.

Evans, K. (2012). The redox budget of subduction zones. *Earth-Science Reviews*, *113*, 11–32.

Evans, K., & Powell, R. (2015). The effect of subduction on the sulfur, carbon, and redox budget of lithospheric mantle. *Journal of Metamorphic Geology*, *33*, 649–670.

Evans, K., Tomkins, A., Cliff, J., & Fiorentini, M. (2014). Insights into subduction zone sulfur recycling from isotopic analysis of eclogite-hosted sulfides. *Chemical Geology*, *365*, 1–19.

Farquhar, J., Bao, H., & Thiemens, M. (2000). Atmospheric influence of Earth's earliest sulfur cycle. *Science*, *289*, 756–758.

Farquhar, J., Cliff, J., Zerkle, A. L., Kamyshny, A., Poulton, S. W., Claire, M., … Harms, B. (2013). Pathways for Neoarchean pyrite formation constrained by mass-independent sulfur isotopes. *Proceedings of the National Academy of Sciences*, *110*, 17638–17643.

Farquhar, J., Savarino, J., Airieau, S., & Thiemens, M. H. (2001). Observation of wavelength-sensitive mass-independent sulfur isotope effects during SO2 photolysis: implications for the early atmosphere. *Journal of Geophysical Research: Planets (1991–2012)*, *106*, 32829–32839.

Farquhar, J., & Wing, B. A. (2003). Multiple sulfur isotopes and the evolution of the atmosphere. *Earth and Planetary Science Letters*, *213*, 1–13.

Farquhar, J., Wing, B., Mckeegan, K., Harris, J., Cartigny, P., & Thiemens, M. (2002). Mass-independent sulfur of inclusions in diamond and sulfur recycling on early Earth. *Science*, *298*, 2369–2372.

Fedo, C. M., & Eriksson, K. A. (1995). Geologic setting and ideas concerning the origin of the iron-ore deposits at Buhwa, Zimbabwe. In T. G. Blenkinsop, & P. L. Tromp (Eds.), *Sub-Saharan Economic Geology*, *1993*, (pp. 43–53). Rotterdam: A.A. Balkema.

Fike, D. A., Bradley, A. S., & Rose, C. V. (2015). Rethinking the ancient sulfur cycle. *Annual Review of Earth and Planetary Sciences*, *43*, 593–622.

Fischer, W. W., Fike, D. A., Johnson, J. E., Raub, T. D., Guan, Y., Kirschvink, J. L., & Eiler, J. M. (2014). SQUID–SIMS is a useful approach to uncover primary signals in the Archean sulfur cycle. *Proceedings of the National Academy of Sciences*, *111*, 5468–5473.

Fischer, W., Schroeder, S., Lacassie, J., Beukes, N., Goldberg, T., Strauss, H., … Knoll, A. (2009). Isotopic constraints on the Late Archean carbon cycle from the Transvaal Supergroup along the western margin of the Kaapvaal Craton, South Africa. *Precambrian Research*, *169*, 15–27.

Galer, S. J., & Mezger, K. (1998). Metamorphism, denudation and sea level in the Archean and cooling of the Earth. *Precambrian Research*, *92*, 389–412.

Gallagher, M., Turner, E. C., & Kamber, B. S. (2015). In situ trace metal analysis of Neoarchaean – Ordovician shallow-marine microbial-carbonate-hosted pyrites. *Geobiology*, *13*, 316–339.

Giacometti, F., Evans, K. A., Rebay, G., Cliff, J., Tomkins, A. G., Rossetti, P., … Adams, D. T. (2014). Sulfur isotope evolution in sulfide ores from Western Alps: Assessing the influence of subduction-related metamorphism. *Geochemistry, Geophysics, Geosystems*, *15*, 3808–3829.

Grotzinger, J. P., & Kasting, J. F. (1993). New constraints on Precambrian ocean composition. *The Journal of Geology*, *101*, 235–243.

Guo, Q., Strauss, H., Kaufman, A. J., Schröder, S., Gutzmer, J., Wing, B., … Kim, S.-T. (2009). Reconstructing Earth's surface oxidation across the Archean-Proterozoic transition. *Geology*, *37*, 399–402.

Habicht, K. S., Gade, M., Thamdrup, B., Berg, P., & Canfield, D. E. (2002). Calibration of sulfate levels in the Archean ocean. *Science*, *298*, 2372–2374.

Hälbich, I. W. (1992). The Cape Fold Belt Orogeny: State of the art 1970s-1980s. In M. J. de Wit & I. G. D. Ransome (Eds.), *Inversion tectonics of the Cape Fold Belt, Karoo and Cretaceous Basins of Southern Africa* (pp. 141–158). Rotterdam: Balkema.

Hälbich, I. W., Lamprecht, D., Altermann, W., & Horstmann, U. (1992). A carbonate-banded iron formation transition in the Early Protorezoicum of South Africa. *Journal of African Earth Sciences (and the Middle East)*, *15*, 217–236.

Halevy, I. (2013). Production, preservation, and biological processing of mass-independent sulfur isotope fractionation in the Archean surface environment. *Proceedings of the National Academy of Sciences*, *110*, 17644–17649.

Halevy, I., Johnston, D. T., & Schrag, D. P. (2010). Explaining the structure of the Archean mass-independent sulfur isotope record. *Science*, *329*, 204–207.

Hofmann, H. (2000). Archean stromatolites as microbial archives. In R. Riding & S. M. Awramik (Eds.), *Microbial sediments* (pp. 315–327). Heidelberg: Springer Berlin Heidelberg

Hofmann, A., Bekker, A., Rouxel, O., Rumble, D., & Master, S. (2009). Multiple sulphur and iron isotope composition of detrital pyrite in Archaean sedimentary rocks: A new tool for provenance analysis. *Earth and Planetary Science Letters*, *286*, 436–445.

Holland, H. D. (1984). *The chemical evolution of the atmosphere and oceans*. Princeton, NJ: Princeton University Press.

Imai, A., Listanco, E., & Fujii, T. (1993). Petrologic and sulfur isotopic significance of highly oxidized and sulfur-rich magma of Mt. Pinatubo, Philippines. *Geology*, *21*, 699–702.

Izon, G., Zerkle, A. L., Zhelezinskaia, I., Farquhar, J., Newton, R. J., Poulton, S. W., … Claire, M. W. (2015). Multiple oscillations in Neoarchaean atmospheric chemistry. *Earth and Planetary Science Letters*, *431*, 264–273.

Jégo, S., & Dasgupta, R. (2013). Fluid-present melting of sulfide-bearing ocean-crust: Experimental constraints on the transport of sulfur from subducting slab to mantle wedge. *Geochimica et Cosmochimica Acta*, *110*, 106–134.

Kamber, B. S. (2010). Archean mafic–ultramafic volcanic landmasses and their effect on ocean–atmosphere chemistry. *Chemical Geology*, *274*, 19–28.

Kamber, B. S. (2015). The evolving nature of terrestrial crust from the Hadean, through the Archaean, into the Proterozoic. *Precambrian Research*, *258*, 48–82.

Kamber, B. S., Collerson, K. D., Moorbath, S., & Whitehouse, M. J. (2003). Inheritance of early Archaean Pb-isotope variability from long-lived Hadean protocrust. *Contributions to Mineralogy and Petrology*, *145*, 25–46.

Kamber, B. S., & Webb, G. E. (2001). The geochemistry of late Archaean microbial carbonate: Implications for ocean chemistry and continental erosion history. *Geochimica et Cosmochimica Acta*, *65*, 2509–2525.

Kamber, B. S., Webb, G. E., & Gallagher, M. (2014). The rare earth element signal in Archaean microbial carbonate: Information on ocean redox and biogenicity. *Journal of the Geological Society*, *171*, 745–763.

Kamber, B., & Whitehouse, M. (2007). Micro-scale sulphur isotope evidence for sulphur cycling in the late Archean shallow ocean. *Geobiology*, *5*, 5–17.

Keller, C. B., & Schoene, B. (2012). Statistical geochemistry reveals disruption in secular lithospheric evolution about 2.5 [thinsp] Gyr ago. *Nature*, *485*, 490–493.

Klein, C., & Beukes, N. J. (1989). Geochemistry and sedimentology of a facies transition from limestone to iron-formation deposition in the early Proterozoic Transvaal Supergroup, South Africa. *Economic Geology*, *84*, 1733–1774.

Konhauser, K. O., Pecoits, E., Lalonde, S. V., Papineau, D., Nisbet, E. G., Barley, M. E., … Kamber, B. S. (2009). Oceanic nickel depletion and a methanogen famine before the Great Oxidation Event. *Nature*, *458*, 750–753.

Konhauser, K. O., Robbins, L. J., Pecoits, E., Peacock, C., Kappler, A., & Lalonde, S. V. (2015). The Archean Nickel Famine Revisited. *Astrobiology*, *15*, 804–815.

Large, R. R., Halpin, J. A., Danyushevsky, L. V., Maslennikov, V. V., Bull, S. W., Long, J. A., … Sack, P. J. (2014). Trace element content of sedimentary pyrite as a new proxy for deep-time ocean–atmosphere evolution. *Earth and Planetary Science Letters*, *389*, 209–220.

Ling, H., Burton, K., O'nions, R., Kamber, B., Von Blanckenburg, F., Gibb, A., & Hein, J. (1997). Evolution of Nd and Pb isotopes in Central Pacific seawater from ferromanganese crusts. *Earth and Planetary Science Letters*, *146*, 1–12.

Mandeville, C. W., Webster, J. D., Tappen, C., Taylor, B. E., Timbal, A., Sasaki, A., … Bacon, C. R. (2009). Stable isotope and petrologic evidence for open-system degassing during the climactic and pre-climactic eruptions of Mt. Mazama, Crater Lake, Oregon. *Geochimica et Cosmochimica Acta*, *73*, 2978–3012.

Marx, S. K., Kamber, B. S., Mcgowan, H. A., & Zawadzki, A. (2010). Atmospheric pollutants in alpine peat bogs record a detailed chronology of industrial and agricultural development on the Australian continent. *Environmental Pollution*, *158*, 1615–1628.

Métrich, N., Schiano, P., Clocchiatti, R., & Maury, R. C. (1999). Transfer of sulfur in subduction settings: An example from Batan Island (Luzon volcanic arc, Philippines). *Earth and Planetary Science Letters*, *167*, 1–14.

Minikin, A., Legrand, M., Hall, J., Wagenbach, D., Kleefeld, C., Wolff, E., … Ducroz, F. (1998). Sulfur-containing species (sulfate and methanesulfonate) in coastal Antarctic aerosol and precipitation. *Journal of Geophysical Research: Atmospheres*, *103*, 10975–10990.

Mloszewska, A. M., Pecoits, E., Cates, N. L., Mojzsis, S. J., O'neil, J., Robbins, L. J., & Konhauser, K. O. (2012). The composition of Earth's oldest iron formations: The Nuvvuagittuq Supracrustal Belt (Québec, Canada). *Earth and Planetary Science Letters*, *317*, 331–342.

Nelson, D., Trendall, A., & Altermann, W. (1999). Chronological correlations between the Pilbara and Kaapvaal cratons. *Precambrian Research*, *97*, 165–189.

Nozaki, Y., Thomson, J., & Turekian, K. (1976). The distribution of 210 Pb and 210 Po in the surface waters of the Pacific Ocean. *Earth and Planetary Science Letters*, *32*, 304–312.

Nozaki, Y., & Tsunogai, S. (1976). 226Ra, 210Pb and 210Po disequilibria in the Western North Pacific. *Earth and Planetary Science Letters*, *32*, 313–321.

Ohmoto, H., & Felder, R. P. (1987). Bacterial activity in the warmer, sulphate-bearing, Archaean oceans. *Nature*, *328*, 244–246.

Ohmoto, H., Watanabe, Y., Ikemi, H., Poulson, S. R., & Taylor, B. E. (2006). Sulphur isotope evidence for an oxic Archaean atmosphere. *Nature*, *442*, 908–911.

Ono, S., Beukes, N. J., Rumble, D., & Fogel, M. L. (2006). Early evolution of atmospheric oxygen from multiple-sulfur and carbon isotope records of the 2.9 Ga Mozaan Group of the Pongola Supergroup, Southern Africa. *South African Journal of Geology*, *109*, 97–108.

Ono, S., Eigenbrode, J. L., Pavlov, A. A., Kharecha, P., Rumble Iii, D., Kasting, J. F., & Freeman, K. H. (2003). New insights into Archean sulfur cycle from mass-independent sulfur isotope records from the Hamersley Basin, Australia. *Earth and Planetary Science Letters*, *213*, 15–30.

Oppenheimer, C., Scaillet, B., & Martin, R. S. (2011). Sulfur degassing from volcanoes: Source conditions, surveillance, plume chemistry and earth system impacts. *Reviews in Mineralogy and Geochemistry*, *73*, 363–421.

Pallister, J. S., Hoblitt, R. P., Meeker, G. P., Knight, R. J., & Siems, D. F. (1996). Magma mixing at Mount Pinatubo: Petrographic and chemical evidence from the 1991 deposits. In C. G. Newhall & R. S. Punongbayan (Eds.), *Fire and Mud: Eruptions and Lahars of Mount Pinatubo, Philippines* (pp. 687–732). Seattle, WA: University of Washington Press.

Pallister, J. S., Hoblitt, R. P., & Reyes, A. G. (1992). A basalt trigger for the 1991 eruptions of Pinatubo volcano? *Nature*, *356*, 426–428.

Papineau, D., Mojzsis, S., Coath, C., Karhu, J., & Mckeegan, K. (2005). Multiple sulfur isotopes of sulfides from sediments in the aftermath

of Paleoproterozoic glaciations. *Geochimica et Cosmochimica Acta*, *69*, 5033–5060.

Paris, G., Adkins, J. F., Sessions, A. L., Webb, S. M., & Fischer, W. W. (2014). Neoarchean carbonate–associated sulfate records positive Δ33S anomalies. *Science*, *346*, 739–741.

Pasteris, J. D. (1996). Mount Pinatubo volcano and "negative" porphyry copper deposits. *Geology*, *24*, 1075–1078.

Patterson, C. C. (1965). Contaminated and natural lead environments of man. *Archives of Environmental Health: An International Journal*, *11*, 344–360.

Pavlov, A., & Kasting, J. (2002). Mass-independent fractionation of sulfur isotopes in Archean sediments: Strong evidence for an anoxic Archean atmosphere. *Astrobiology*, *2*, 27–41.

Philippot, P., Van Zuilen, M., & Rollion-Bard, C. (2012). Variations in atmospheric sulphur chemistry on early Earth linked to volcanic activity. *Nature Geoscience*, *5*, 668–674.

Plank, T., & Langmuir, C. H. (1998). The chemical composition of subducting sediment and its consequences for the crust and mantle. *Chemical Geology*, *145*, 325–394.

Reinhard, C. T., Planavsky, N. J., & Lyons, T. W. (2013). Long-term sedimentary recycling of rare sulphur isotope anomalies. *Nature*, *497*, 100–103.

Rouxel, O. J., Bekker, A., & Edwards, K. J. (2005). Iron isotope constraints on the Archean and Paleoproterozoic ocean redox state. *Science*, *307*, 1088–1091.

Savarino, J., Romero, A., Cole-Dai, J., Bekki, S., & Thiemens, M. (2003). UV induced mass-independent sulfur isotope fractionation in stratospheric volcanic sulfate. *Geophysical Research Letters*, *30*, 2131.

Schaule, B. K., & Patterson, C. C. (1981). Lead concentrations in the northeast Pacific: Evidence for global anthropogenic perturbations. *Earth and Planetary Science Letters*, *54*, 97–116.

Schopf, J. W., Kudryavtsev, A. B., Czaja, A. D., & Tripathi, A. B. (2007). Evidence of Archean life: Stromatolites and microfossils. *Precambrian Research*, *158*, 141–155.

Shen, Y., Farquhar, J., Masterson, A., Kaufman, A. J., & Buick, R. (2009). Evaluating the role of microbial sulfate reduction in the early Archean using quadruple isotope systematics. *Earth and Planetary Science Letters*, *279*, 383–391.

Shirey, S. B., & Richardson, S. H. (2011). Start of the Wilson cycle at 3 Ga shown by diamonds from subcontinental mantle. *Science*, *333*, 434–436.

Sumner, D. Y. (1997). Late Archean calcite-microbe interactions; two morphologically distinct microbial communities that affected calcite nucleation differently. *Palaios*, *12*, 302–318.

Sumner, D. Y., & Bowring, S. A. (1996). U·Pb geochronologic constraints on deposition of the Campbellrand Subgroup, Transvaal Supergroup, South Africa. *Precambrian Research*, *79*, 25–35.

Thurston, P., Ayer, J., Goutier, J., & Hamilton, M. (2008). Depositional gaps in Abitibi greenstone belt stratigraphy: A key to exploration for syngenetic mineralization. *Economic Geology*, *103*, 1097–1134.

Thurston, P., Kamber, B., & Whitehouse, M. (2012). Archean cherts in banded iron formation: insight into Neoarchean ocean chemistry and depositional processes. *Precambrian Research*, *214*, 227–257.

Ulrich, T., Long, D., Kamber, B., & Whitehouse, M. (2011). In situ trace element and sulfur isotope analysis of pyrite in a paleoproterozoic gold placer deposit, Pardo and Clement Townships, Ontario, Canada. *Economic Geology*, *106*, 667–686.

Van De Flierdt, T., Frank, M., Halliday, A. N., Hein, J. R., Hattendorf, B., Günther, D., & Kubik, P. W. (2003). Lead isotopes in North Pacific deep water–implications for past changes in input sources and circulation patterns. *Earth and Planetary Science Letters*, *209*, 149–164.

Von Blanckenburg, F., O'Nions, R., & Heinz, J. (1996). Distribution and sources of pre-anthropogenic lead isotopes in deep ocean water from Fe Mn crusts. *Geochimica et cosmochimica acta*, *60*, 4957–4963.

Wagenbach, D., Ducroz, F., Mulvaney, R., Keck, L., Minikin, A., Legrand, M., … Wolff, E. W. (1998). Sea-salt aerosol in coastal Antarctic regions. *Journal of Geophysical Research: Atmospheres*, *103*, 10961–10974.

Walker, J. C., & Brimblecombe, P. (1985). Iron and sulfur in the pre-biologic ocean. *Precambrian Research*, *28*, 205–222.

Whitehouse, M. J. (2013). Multiple sulfur isotope determination by SIMS: Evaluation of reference sulfides for Δ33S with observations and a case study on the determination of Δ36S. *Geostandards and Geoanalytical Research*, *37*, 19–33.

Williford, K., Ushikubo, T., Lepot, K., Kitajima, K., Hallmann, C., Spicuzza, M., … Valley, J. (2016). Carbon and sulfur isotopic signatures of ancient life and environment at the microbial scale: Neoarchean shales and carbonates. *Geobiology*, *14*, 1472–4669.

Wu, J., & Boyle, E. A. (1997). Lead in the western North Atlantic Ocean: Completed response to leaded gasoline phaseout. *Geochimica et Cosmochimica Acta*, *61*, 3279–3283.

Zegers, T., De Wit, M., Dann, J., & White, S. (1998). Vaalbara, Earth's oldest assembled continent? A combined structural, geochronological, and palaeomagnetic test. *Terra Nova*, *10*, 250–259.

Zeh, A., Wilson, A. H., & Ovtcharova, M. (2016). Source and age of upper Transvaal Supergroup, South Africa: Age-Hf isotope record of zircons in Magaliesberg quartzite and Dullstroom lava, and implications for Paleoproterozoic (2.5–2.0 Ga) continent reconstruction. *Precambrian Research*, *278*, 1–21.

Zerkle, A. L., Claire, M., Domagal-Goldman, S. D., Farquhar, J., & Poulton, S. W. (2012). A bistable organic-rich atmosphere on the Neoarchaean Earth. *Nature Geoscience*, *5*, 359–363.

Zhelezinskaia, I., Kaufman, A. J., Farquhar, J., & Cliff, J. (2014). Large sulfur isotope fractionations associated with Neoarchean microbial sulfate reduction. *Science*, *346*, 742–744.

SUPPORTING INFORMATION

Additional Supporting Information may be found online in the supporting information tab for this article.

How to cite this article: Gallagher M, Whitehouse MJ, Kamber BS. The Neoarchaean surficial sulphur cycle: An alternative hypothesis based on analogies with 20th-century atmospheric lead. *Geobiology*. 2017;00:1–16. https://doi.org/10.1111/gbi.12234